



Title	Study on the mechanism of stochastic defects generation in EUV lithography
Author(s)	春本, 将彦
Citation	大阪大学, 2023, 博士論文
Version Type	VoR
URL	https://doi.org/10.18910/91914
rights	
Note	

The University of Osaka Institutional Knowledge Archive : OUKA

<https://ir.library.osaka-u.ac.jp/>

The University of Osaka

Doctoral Dissertation

**Study on the mechanism of stochastic defects generation
in EUV lithography**

(極端紫外線リソグラフィにおける
確率的欠陥の発生機構に関する研究)

Masahiko Harumoto

December 2022

Graduate School of Engineering,
Osaka University

Preface

The work of this thesis has been carried out under the guidance of Professor Takahiro Kozawa at Development of Beam Materials Science, the Institute of Scientific and Industrial Research, Osaka University.

The objectives of this work are to develop the semiconductor coat-develop process module by clarifying the mechanism of randomly generated stochastic defects in EUV lithography.

Contents

Chapter 1	General introduction	1
1-1.	Challenges of extreme ultraviolet lithography in semiconductor manufacturing	3
1-2.	Stochastic defects in EUV lithography	4
1-3.	Photoresist polymer and alkaline developer materials	5
1-4.	Objectives	7
	Reference	8
Chapter 2	Pattern collapse mitigation by controlling atmosphere during development process for semiconductor lithography	9
2-1.	Introduction	11
2-2.	Experimental	12
2-3.	Results and discussion	14
2-4.	Conclusion	19
	References	19
Chapter 3	Dependence of photoresist dissolution dynamics in alkaline developers on alkyl chain length of tetraalkylammonium hydroxide	23
3-1.	Introduction	25
3-2.	Experimental	26
3-3.	Results and discussion	28
3-4.	Conclusion	33
	References	34
Chapter 4	Stochastic defect generation depending on tetraalkylhydroxide aqueous developers in extreme ultraviolet lithography	37
4-1.	Introduction	39
4-2.	Experimental conditions	40
4-3.	Results and discussion	42
4-4.	Conclusion	48
	References	48
Chapter 5	Conclusions	51
	List of publications	56

Chapter 1

General introduction

1-1. Challenges of extreme ultraviolet lithography in semiconductor manufacturing

Semiconductor integrated circuits (IC) play a major role in the fields of information processing and communication technologies, and are now widely used. As forecasted by Moore's Law,¹⁾ the density of ICs continues to increase every year. Such advancements translate to dramatic growth in information processing capacity, a significant factor in the spread and expansion of information processing devices such as personal computers and in recent years, smart phones. Since the spread of cell phones in the 1980s, information communication technologies have continued to progress forward, starting with the first-generation mobile communication system (1G) and now, with transmitting signals up to 20 Gb/s, fifth-generation mobile communication system (5G). Cutting edge ICs are needed to instantly process large volumes of transmitted and received signals. This further pushes IC integration / manufacturing to much more stringent requirements every year.^{2,3)}

Increasing IC integration means increasing the number (density) of transistors fabricated in a given area (in the IC) through miniaturization. In IC manufacturing, there are various processes such as cleaning, film deposition, lithography, etching and doping that are performed in numerous repeating cycles. Lithography is the IC manufacturing process step where the structure designs / patterns for gates and interconnections are transferred to substrates. This is also the first step of miniaturization or pitch scaling in IC manufacturing. Typical pitch scaling techniques in lithography are; shorter wavelength (λ) of exposure source utilized to transfer patterns to substrates, higher numerical aperture of projection lens in the exposure tool utilized, higher resolution of photoresist polymer and so on. Extreme ultraviolet (EUV) lithography ($\lambda = 13.5$ nm), the current leading edge lithographic technology, is now starting to be utilized in the mass production of ICs.⁴⁻⁶⁾ However, to fully take advantage of the extremely fine, sub-10 nm pitch scaling through this technology, the challenge of understanding and mitigating the major issue of stochastic pattern defects needs to be seriously considered.^{7,8)}

1-2. Stochastic defects in EUV lithography

Stochastic defects are randomly generated type of defects that pose as a possibly major issue in EUV lithography. Figure 1-1 indicates one such stochastic defect; (a) pattern collapse which occurs when the ratio of height to line width exceeds a certain level. Another is (b) ‘closed hole’ defects which occur when the pattern size falls below a certain level.

Lithography is composed of several processes; photoresist coating, pattern exposure,

post exposure baking, and lastly developing. Each of these processes are perceived to have an effect on the stochastic defect generation. Figure 1-2 shows a schematic cross-sectional view of the photoresist for each process step. The first step is the photoresist coating. It is considered that photoacid generators (PAG) in a photoresist film are uniformly distributed macroscopically, however, microscopically distances between PAGs are not uniform and they are normally distributed. This normally distributed distance is one of the causes of stochastic defect generation. Along with PAGs, photoacid diffusion inhibitors (i.e. quenchers) are also considered to be unevenly distributed across the film, but for the sake of simplicity, only the PAGs are considered in this diagram. The second step is pattern exposure. PAGs are irradiated by the exposure light and generate acid in the photoresist film. The exposure light intensity is normally distributed, furthermore, the number of photons per unit volume in EUV light is relatively much lower than previous lithographic technologies (10 to 100 times lower than in ArF light). The smaller number of unevenly distributed photons is also considered to be one of the causes of the stochastic defects generation.⁹⁾ The third step is the post exposure baking which amplifies and diffuses the acid generated by the exposure light, enhancing the deprotection reaction of the photoresist polymer. The acid diffusion length by post exposure baking is also not uniform and is of normal distribution. For this reason, it is also considered that normally distributed diffusion length causes stochastic defects. The last step is developing. The deprotected photoresist dissolves in developer solution at a uniform dissolution rate as a bulk film. However, for every microscopic developer molecule, the photoresist dissolution rate has a normal distribution, another

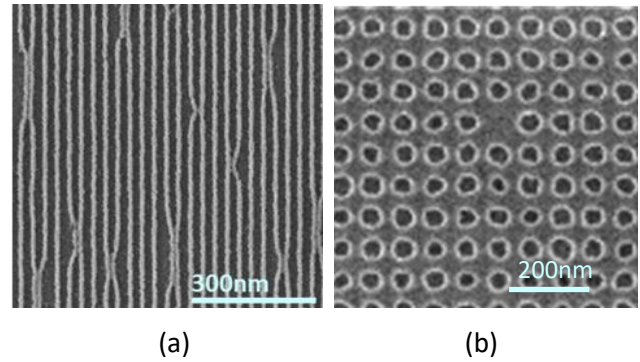


Fig. 1-1 SEM images showing EUV stochastic defects: (a) ‘pattern collapse’ on 32 nm-pitch line-and-space photoresist patterns and (b) ‘closed hole’ on 42 nm-hole photoresist patterns with 70 nm-pitch.

cause of stochastic defect generation.

As mentioned earlier, stochastic pattern defect generation in photoresists are the combination of several factors in the various steps of lithography. To summarize; PAG locations in coating film, the exposure light intensity and associated acid generation distribution, the acid diffusion length in post exposure baking and photoresist dissolution rate in development are uniformly distributed macroscopically throughout the system, but have a normal distribution microscopically, so that they are combined to generate stochastic defects in the photoresist pattern.

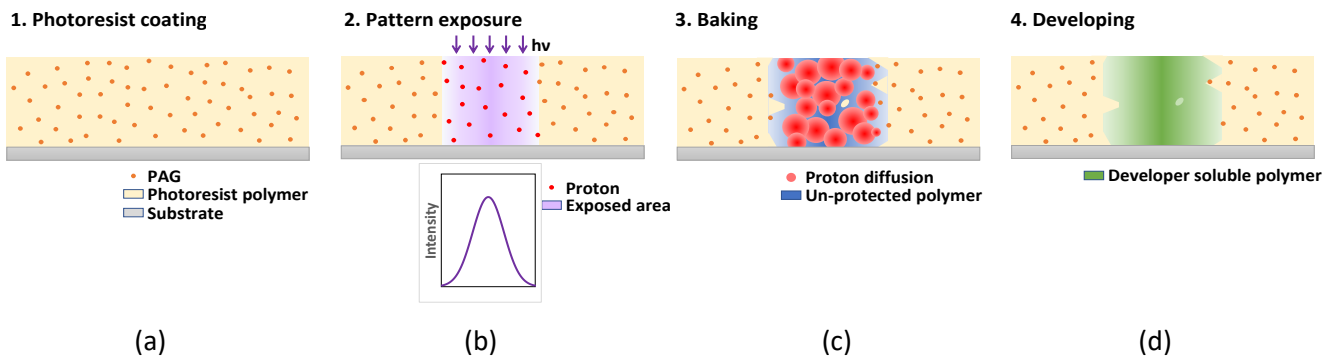


Fig. 1-2 Sources of stochastic defects in each lithography process step: (a) PAG distribution after coating, (b) acid generation by exposure light and its intensity in exposed area, (c) proton diffusion with baking and (d) solubility/insolubility of photoresist to developer.

1-3. Photoresist polymer and alkaline developer materials

Figure 1-3 shows the three typical types of photoresist polymer utilized in these experiments. These types of photoresist polymers are the commonly applied materials in lithography; polyhydroxystyrene (PHS) type polymer is utilized for KrF lithography, acryl-type polymer is utilized for ArF lithography, and PHS-acryl hybrid-type polymer is being utilized for EUV lithography. Triphenylsulfonium-trifluoromethanesulfonate (TPS-triflate) was used as a photoacid generator (PAG) and tri-n-octylamine (TOA) was used as a quencher for each photoresist. It is known that the molecular weights of the entanglements for PHS and acrylate polymer were about 30,000 and 20,000, respectively¹⁰. It is considered small enough not to affect the dissolution behavior because the molecular weights are about 7,000 for PHS-type and hybrid-type photoresist and 11,000 for acryl-type photoresist polymer in this study.

Tetramethylammonium hydroxide (TMAH) aqueous solutions is utilized as the standard alkaline developer in the high-volume manufacturing and tetrabutylammonium hydroxide (TBAH) aqueous solutions is being considered as a specific developer for EUV lithography. Figure 1-4 shows four types of alkaline developer utilized in this study, TMAH, tetraethylammonium hydroxide (TEAH), tetrapropylammonium hydroxide (TPAH), and TBAH aqueous solutions, were used. The normality of solutions was adjusted to 0.26 N. The pH of the developers was measured to be roughly the same at around 14.3 to 14.4. Moreover, a simple patterning test (50-nm lines-and-spaces) comparing the four types of developers on processing the PHS-type photoresist reveal that regardless of developer solution, there was no significant difference in the measured line width (indicated here as critical dimension or CD) with respect to exposure dose (fig. 1-5). This implies that the various results obtained here can be primarily attributed to the differences in developer characteristics (not differences photon counts due to changes in exposure dose).

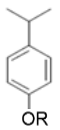
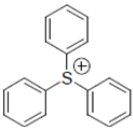
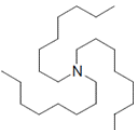
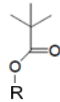
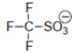
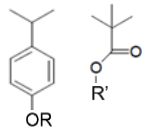
Photoresist	Polymer	PAG	Quencher	Solvent
PHS-type				PGMEA/PGME (60/40)
Acryl-type			TOA	
Hybrid-type				

Fig. 1-3 typical three types of photoresist polymer.

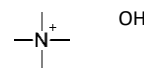
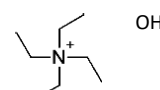
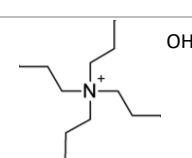
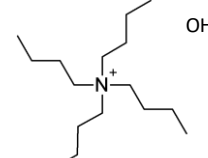
Developer name	Chemical structure
TMAH (Tetramethylammonium Hydroxide)	
TEAH (Tetraethylammonium Hydroxide)	
TPAH (Tetrapropylammonium Hydroxide)	
TBAH (Tetrabutylammonium Hydroxide)	

Fig. 1-4 Tetraalkylammonium hydroxide developers used in this study.

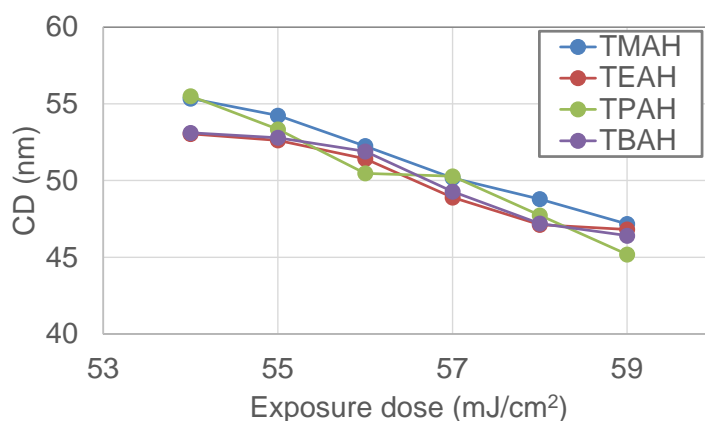


Fig. 1-5 50-nm lines-and-spaces pattern CD at various exposure doses by each alkaline developer.

1-4. Objectives

The objectives in this study were to clarify the mechanism of randomly generated stochastic defects in EUV lithography. In Chapter 1, the objective was to verify pattern collapse mitigation by ArF immersion photoresist pattern with 140 nm film thickness and to clarify its mechanism through the physical approach of reducing atmosphere pressure during and after the development process. Chapter 2 was designed to clarify the photoresist dissolution dynamics of three typical EUV photoresists in

four types of alkaline developers with different alkyl chain lengths. In Chapter 3, hole patterns were fabricated using the same photoresists and developers in Chapter 2, with the objective of clarifying the mechanism of randomly generated closed and open hole defects in terms of dissolution dynamics.

References

- 1) G. E. Moore, IEEE SSCS NEWSLETTER, **Vol.38**, Number8 pp.114 ff. (1965).
- 2) Ministry of Economy, Trade and Industry in Japan, ‘The 4th Semiconductor and Digital Industry Strategy Review Meeting’ (2021), [in Japanese].
[<https://www.meti.go.jp/press/2021/06/20210630001/20210630001-1.pdf>]
- 3) Ministry of Education, Culture, Sports, Science and Technology in Japan, Council for Science, Technology and Innovation meeting, ‘Results of the preliminary evaluation of R&D proposals related to environmental energy science and technology (2)’ (2021), [in Japanese].
[https://www.mext.go.jp/component/b_menu/shingi/toushin/___icsFiles/afieldfile/2018/10/15/1409970_05.pdf]
- 4) X. Chen, A. Gabor, P. Samudrala, S. Meyers, E. Hosler, R. Johnson, and N. Felix, Proc. SPIE **10143**, 10143F-1 (2017).
- 5) G. Yeap, S. S. Lin, Y. M. Chen, S. M. Jang et al., IEEE IEDM **879**, 3671 (2019).
- 6) T.Y.J. Chang, Y.H. Chen, W.M. Chan, H. Cheng, P.S. Wang, Y. Lin, H. Fujiwara, R. Lee, H.J. Liao, P.W. Wang, G. Yeap, and Q. Li, IEEE J. Solid-state Circuits, **56**, 1, 179-187 (2021).
- 7) T. Kozawa, J. J. Santillan, and T. Itani, Jpn. J. Appl. Phys. **52**, 076502 (2013).
- 8) P. D. Bisschop, J. V. Kerkhove, J. Mailfert, A. V. Pret, and J. Biafore, Proc. SPIE **9048**, 904809 (2014).
- 9) J. J. Biafore, M. D. Smith, C. A. Mack, J. W. Thackeray, R. Gronheid, S A. Roberson, T. Graves, and D. Blankenship, Proc. SPIE **7273**, 727343 (2009).
- 10) Roger S. Porter and Julian F. Johnson, Chemical Reviews, Vol. **66**, Number 1, 1-27 (1966).

Chapter 2

**Pattern collapse mitigation by controlling atmosphere
during development process for semiconductor lithography**

2-1. Introduction

The resolution of photoresist materials used for semiconductor lithography has been improved to meet the market demands of highly integrated semiconductor devices. The resolution of photoresist materials was often limited by the pattern collapse. The photoresist pattern collapse at post-development is one of the traditional issues in the lithography process and still important. This has been true in every

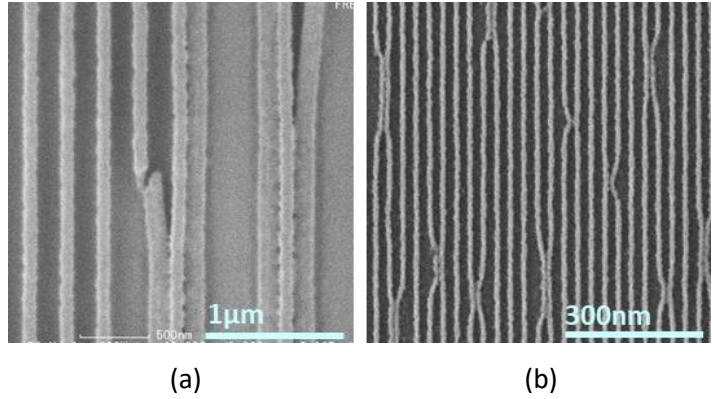


Fig. 2-1 SEM images showing pattern collapse: (a) 260 nm pitch line-and-space photoresist patterns and (b) 32 nm pitch line-and-space photoresist patterns.

generation of photoresists; i-line, KrF, ArF, ArF immersion, and recently EUV.¹⁻⁴⁾ Figure 2-1 shows the scanning electron microscopy (SEM) images of photoresist pattern collapse. Figure 2-1(a) shows the KrF photoresist pattern with 260 nm pitch and Fig. 2-1(b) shows EUV photoresist pattern with 32 nm pitch.

The cause of pattern collapse has been investigated.^{5,6)} The schematics of the capillary force on the photoresist pattern are shown in Fig. 2-2. The differential pressure P between the atmosphere pressure $P_{atmosphere}$ and the rinsing liquid pressure P_{rinse} is expressed as

$$P = P_{atmosphere} - P_{rinse} = \frac{2\gamma \cos \theta}{d}, \quad (1)$$

where γ is the surface tension of rinsing liquid, θ is the contact angle with the photoresist pattern and the rinsing liquid, and d is the width of space between line patterns. The pattern collapse is caused by the tensile stress arising during the rinsing and drying in the development process. The tensile stress σ is expressed as

$$\sigma = 3P \left(\frac{H}{L}\right)^2 = \frac{6\gamma \cos \theta}{d} \left(\frac{H}{L}\right)^2, \quad (2)$$

where H is the pattern height and L is the pattern width. The main factors of tensile stress are the surface tension of rinsing liquid and the pattern structure (height, line width, and space width). The photoresist pattern collapse will occur when the tensile stress σ caused by the rinsing liquid exceeds the adhesion force between photoresist patterns and the substrate. Many studies have been carried out to prevent the photoresist pattern collapse. The improvement of rinsing liquids, for example, by adding

surfactants, has been investigated.⁷⁻⁹⁾ The alternative rinsing materials such as supercritical fluids were examined to reduce the surface tension.¹⁰⁻¹²⁾ Freeze-drying process,¹³⁾ dry development rinse process (DDRP),¹⁴⁾ laser dry development,¹⁵⁾ and thermal development¹⁶⁾ are alternative processes for the prevention of pattern collapse. From the viewpoints of photoresist materials, the improvement of mechanical properties by the modification of resist materials has been reported to prevent the pattern collapse.¹⁷⁻¹⁸⁾ The use of underlayers is effective to prevent the pattern collapse by increasing the adhesion force.^{19,20)} The effects of the developer on the pattern collapse have also been reported.^{21,22)}

In this study, the author focused on the differential pressure for the mitigation of pattern collapse. The differential pressure is proportional to σ as expressed by Eq. (2). Therefore, the photoresist pattern collapse will be mitigated with lower pressure during drying after the deionized water (DIW) rinsing. We attempted to mitigate the photoresist pattern collapse by controlling the atmosphere pressure.

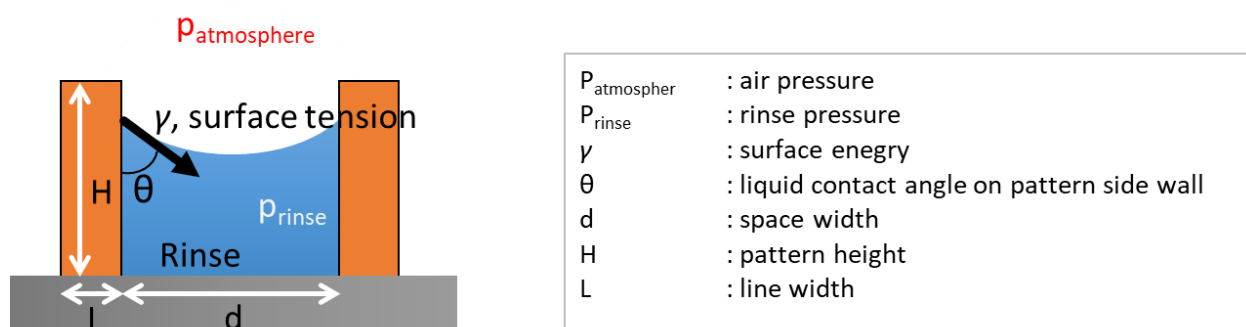


Fig. 2-2 Schematics of the capillary force imposed on photoresist patterns. The differential pressure between the atmosphere pressure $P_{atmosphere}$ and the rinsing liquid pressure P_{rinse} is expressed as Eqs. (1) and (2).

2-2. Experimental

2-2-1. Materials and tools

The bi-layer stack was prepared by spin coating. The bottom layer is an anti-reflective coating (ARC) with 30 nm film thickness that was coated on Si substrate and baked at 205°C in 60 seconds. The top layer is an ArF-immersion photoresist with polymethacrylate backbone polymer with 140 nm film thickness that was coated on the ARC layer and baked at 120 °C in 60 seconds.^{23,24)}

The photoresist patterns were fabricated by ArF immersion technology. Resist processes (coat, bake, etc.) were performed in an in-line coater developer system, SOKUDO DUO coater/developer (SCREEN Semiconductor Solutions), attached to the exposure tool, NXT-1950Ai (ASML), with 1.35 numerical aperture (NA).²⁵⁻²⁷⁾ The development with 0.26 N tetramethylammoniumhydroxide

(TMAH) aqueous developer and rinsing with DIW were carried out. SEM measurements were performed using CG5000 (Hitachi High-Technologies).^{27,28)}

2-2-2. Exposure conditions

There are 633 exposed dies with 10 mm square. The number of columns and rows is 29 at most. This matrix was used for the dose-focus matrix where the focus was varied from -0.70 to $+0.70$ μm and the dose was varied from 16.0 to 44.0 mJ/cm^2 . The critical dimension (CD) at the best focus was used for the photoresist pattern collapse evaluation.

2-2-3. Development process steps

The development process steps are shown in Fig. 2-3. The development process was performed on the film stack after exposure with the ArF-immersion scanner. The developer solution was dispensed to form a puddle on the wafer which was exposed and baked at 90 $^{\circ}\text{C}$ in 60 seconds. After 30 seconds of development time, DIW was then dispensed on to the wafer for 15 seconds (while spinning). The rinsing and drying in the development process were done in a closed chamber, which allowed the control of environmental pressure (the pressure in the chamber, P_c) during rinsing and drying. Hereafter, P_c is expressed by the differential pressure against the atmosphere pressure. Spin drying with rotations from 1000 to 5000 revolutions per minute (rpm) was carried out while monitoring the pressure values in the closed chamber. The photoresist pattern collapse under the atmosphere pressure ($P_c = 0.00$ kN/m^2) was investigated in an open chamber. The photoresist pattern collapse under the negative pressure ($P_c = -0.11, -0.20, \text{ and } -0.32$ kN/m^2) was investigated in the closed chamber.

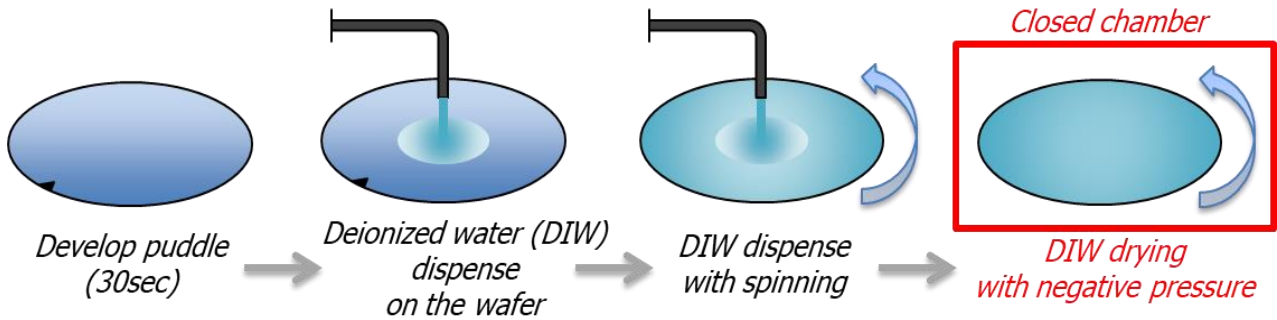


Fig. 2-3 Development process steps: the developer solution is dispensed to form a puddle on the exposed wafer. After 30 seconds of development time, DIW is then dispensed on to the wafer for 15 seconds (while spinning). The rinsing and drying in the development process were done in a closed chamber, which allowed the control of environmental pressure during rinsing and drying.

2-3. Results and discussion

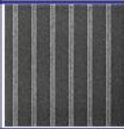

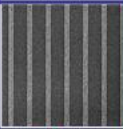
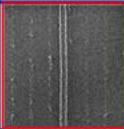

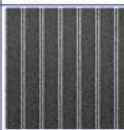
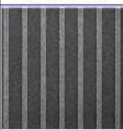

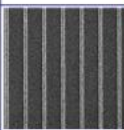
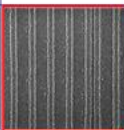
2-3-1. Minimum CD without pattern collapse

The pattern collapse of 130 nm line patterns and 45nm patterns, in which the widths of lines and spaces were designed to be 130 and 156 nm, and 45 and 54 nm, respectively, were investigated. At the best dose for the 130 nm and 45nm lines, the patterns were not collapsed. The limitation of pattern collapse was examined by increasing the exposure dose. Figure 2-4(a) shows the SEM images of pattern collapse for the 130-nm-designed pattern. The minimum CDs without pattern collapse were 56.1 nm under the atmosphere pressure and 50.1 nm under the negative pressure ($P_c = -0.32 \text{ kN/m}^2$). The improvement of approximately 10% was observed, compared with the case under the atmosphere pressure.

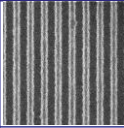
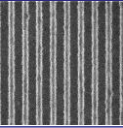
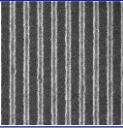
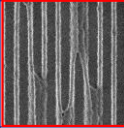
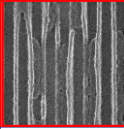
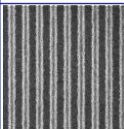
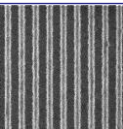
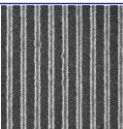
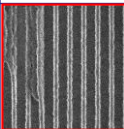
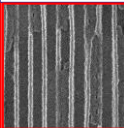
On the other hand, Fig. 2-4(b) shows the SEM images of pattern collapse for the 45-nm-designed pattern. The minimum CDs without pattern collapse were 38.3 nm under the atmosphere and 38.4 nm under the negative pressure ($P_c = -0.32 \text{ kN/m}^2$). There was no improvement of the minimum CD without pattern collapse between the atmosphere and negative pressure conditions.

The relationship between pattern collapse threshold and differential pressure for the 130-nm-designed pattern and 45-nm-designed pattern is shown in Fig. 2-5. The y -axis represents the CD limitation without pattern collapse. The x -axis represents the differential pressure in the chamber, P_c . CDs were measured in the nine areas in the 10 mm square area which was exposed under the same focus and dose conditions and the mean value was plotted in Fig. 2-5 for each condition. The bars of each plot denote the minimum and maximum values among nine measured values. The plotted blue

diamonds represent the result of the 130-nm-designed pattern, and the plotted orange circles represent the result of the 45-nm-designed pattern. The minimum CD without pattern collapse was more improved by decreasing the pressure in the chamber on 130-nm-designed pattern, however, there was no improvement between the atmosphere and negative pressure conditions on 45-nm-designed pattern.

Chamber atmosphere	Designed pattern size	Exposure dose (mJ/cm ²)				
		31.0	32.0	33.0	34.0	35.0
Atmosphere (P_c :0.00 kN/m ²)	130nm 1:1.2					
		59.7nm	58.7nm	56.1nm		
Negative pressure (P_c :-0.32 kN/m ²)	130nm 1:1.2					
		60.0nm	57.7nm	55.9nm	50.1nm	

(a)

Chamber atmosphere	Designed pattern size	Exposure dose (mJ/cm ²)				
		21.0	22.0	23.0	24.0	25.0
Atmosphere (P_c :0.00 kN/m ²)	45nm 1:1.2					
		46.5nm	42.1nm	38.3nm		
Negative pressure (P_c :-0.32 kN/m ²)	45nm 1:1.2					
		47.4nm	42.6nm	38.4nm		

(b)

Fig. 2-4 SEM images of pattern collapse for 130-nm-designed patterns and 45-nm-designed patterns. (a) 130-nm-designed patterns in which the widths of lines and spaces were designed to be 130 and 156 nm, respectively. Exposure dose were 31.0 to 35.0 mJ/cm². The minimum CD was 56.1 nm under the atmosphere and 50.1 nm under the negative pressure, respectively. (b) 45-nm-designed pattern, in which the widths of lines and spaces were designed to be 45 and 54 nm, respectively. Exposure dose were 21.0 to 25.0 mJ/cm². The minimum CD was 38.3 nm under the atmosphere and 38.4 nm under the negative pressure, respectively.

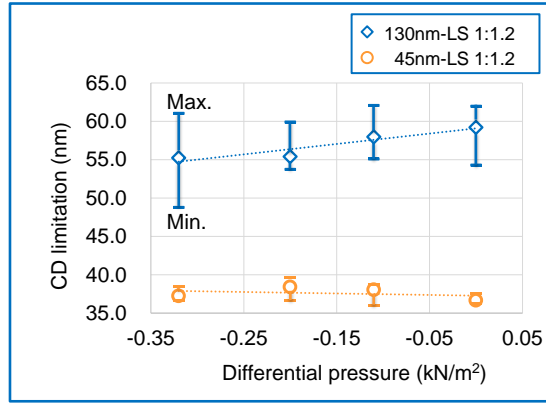


Fig. 2-5 Pattern collapse threshold of 130 nm designed patterns and 45 nm designed patterns for each pressure condition. The y-axis represents the CD limitation without pattern collapse. The x-axis represents the differential pressure in the chamber. The plotted blue diamonds represent the mean of 9 measurement CDs of the 130 nm designed pattern, and the plotted orange circles represent the mean of 9 measurement CDs of the 45 nm designed pattern for each pressure condition. The bars of each plot denote the minimum and maximum values among nine measured values.

2-3-2. Comparison with minimum CD without pattern collapse for 45-130 nm line

The line widths of 45, 60, 90 and 130 nm, in which the line-space ratios are 1:1.2, 1:1.5, and 1:2 respectively, were examined. The summary is shown in Fig. 2-6, including the results described in the previous sections. In this graph, the results of the 1:1.5 and 1:2 patterns are plotted with 0.01 and 0.02 kN/m² offsets from the original differential pressure, respectively, to make each plot easier to see. Table II-I shows a summary of the minimum CDs without patter collapse under the atmosphere pressure and under the negative pressure ($P_c = -0.32$ kN/m²) for the designed 45, 60, 90, and 130 nm line patterns. Comparing both graphs and tables, the minimum CD without pattern collapse was improved by over 5 % on average for 90 and 130 nm lines. However, there was no significant improvement for 45 and 60 nm lines.

Table II-I. Minimum CD without pattern collapse. The designed CDs were 45, 60, 90, and 130 nm.

Chamber atmosphere	Designed CD (nm)	Line CD : Space CD		
		1 : 1.2	1 : 1.5	1 : 2
Atmosphere ($P_c:0.00$ kN/m ²)	130	59.2	62.3	63.2
	90	45.7	45.8	48.1
	60	39.0	40.6	37.9
	45	36.7	37.0	40.3
Negative pressure ($P_c:-0.32$ kN/m ²)	130	55.2	58.8	57.0
	90	40.8	42.1	43.1
	60	37.1	42.0	40.5
	45	37.2	37.7	40.5

(Line CD :nm)

2-3-3. Estimation of maximum tensile stress without pattern collapse and contact angle under negative pressure

The maximum tensile stress σ value was calculated using Eq. (2) and experimental data. Table II-II shows the maximum tensile stress without pattern collapse obtained using the experimental data under the atmosphere, which are listed in Table II-I. The surface tension γ of water is 72.8 mN/m.²⁹⁾ The contact angle was assumed to be $\theta = 60.0$ degrees. The calculated tensile stresses were on the order of 10^6 - 10^7 , which roughly agreed with the reported value.^{30,31)} The maximum tensile stress depended on the pattern duty and the designed line width. The maximum tensile stress should be independent of the pattern duty. This discrepancy is considered to be caused by the overestimation of the pattern height. The loss of film thickness is likely to occur at high duty patterns because the exposure dose was increased beyond the best dose to induce the pattern collapse in this experiment, as mentioned previously. This is also true for the observed dependence of maximum tensile stress on the designed line width. Therefore, the contact angle was calculated using the obtained maximum tensile stress for each pattern to estimate the effect of negative pressure on the contact angle. If the pattern design (line width and duty) is the same, the pattern height at the minimum CD without pattern collapse can be assumed to be approximately the same because the difference of exposure dose is 1 mJ/cm² at most. Table II-III shows the calculated contact angle of DIW during rinsing at $P_c = -0.32$ kN/m². For the 90 and 130 nm line patterns, the contact angle increased approximately by 5 degrees by decreasing the chamber pressure. Although a significant increase was not observed for the 45 and 60 nm line patterns, this is because the dose difference of 1 mJ/cm² did not cause the difference of pattern collapse. It is considered that the negative pressure in this study was not enough large to mitigate the pattern collapse for the designed pattern of 60 nm or less.

Table II-II. Maximum tensile stress obtained through rinsing and drying under the atmosphere pressure. The designed CDs are 45, 60, 90, and 130 nm.

Designed CD (nm)	Line CD : Space CD		
	1 : 1.2	1 : 1.5	1 : 2
130	5.38	4.19	3.28
90	13.5	11.4	8.34
60	30.2	23.7	20.9
45	51.1	41.4	27.8

(10⁶ N/m²)

Table II-III. Calculated contact angle of DIW rinse against the resist pattern sidewall, obtained through rinsing and drying under -0.32 kN/m^2 negative pressure.

Designed CD (nm)	Line CD : Space CD		
	1 : 1.2	1 : 1.5	1 : 2
130	64.2	63.6	66.7
90	66.8	65.2	67.0
60	62.7	61.6	59.2
45	59.3	59.1	59.7

(degrees)

Figure 2-7 shows the capillary effect in the glass tube. For this experiment, a 3 mm inner diameter glass tube and DIW were used. Figure 2-7(a) shows the border of water and air in atmosphere. Figure 2-7(b) shows the border of water and air under negative pressure. It can be observed that the contact angle of water is near 90 degrees under negative pressure. A visible difference can also be seen between atmosphere and negative pressure. A similar phenomenon is considered to have occurred during the rinsing process.³²⁻³⁴⁾ The proposed method is considered to be promising, because it requires no chemical additive,⁷⁻⁹⁾ no additional process,^{14,19,20)} and no special equipment such as a high pressure vessel.¹⁰⁻¹²⁾

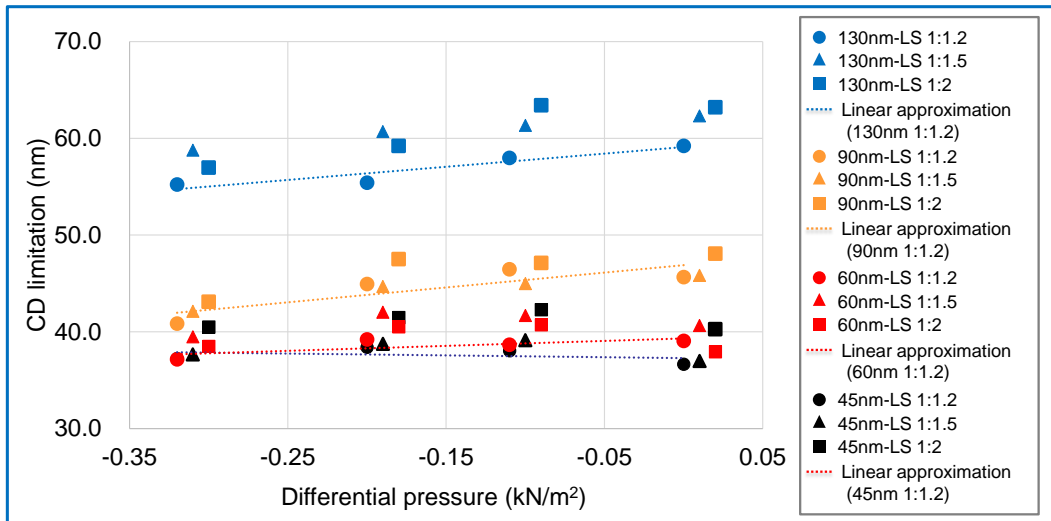


Fig. 2-6 Pattern collapse threshold of 45, 60, 90 and 130 nm designed patterns in which the line-space ratios are 1:1.12, 1:1.5, and 1:2, respectively. The y-axis represents the CD limitation without pattern collapse. The x-axis represents the differential pressure in the chamber. The results of the 1:1.5 and 1:2 patterns are shifted with 0.01 and 0.02 kN/m^2 offsets from the original differential pressure, respectively, to make each plot easier to see. The blue colors represent 130 nm designed patterns, the orange colors represent 90 nm designed patterns, the red colors represent 60 nm designed patterns and the black colors represent 45 nm designed patterns. The circles represent the line-space ratios is 1:1.2, the triangles represent 1:1.5 and the squares represent 1:2 for each size designed pattern.

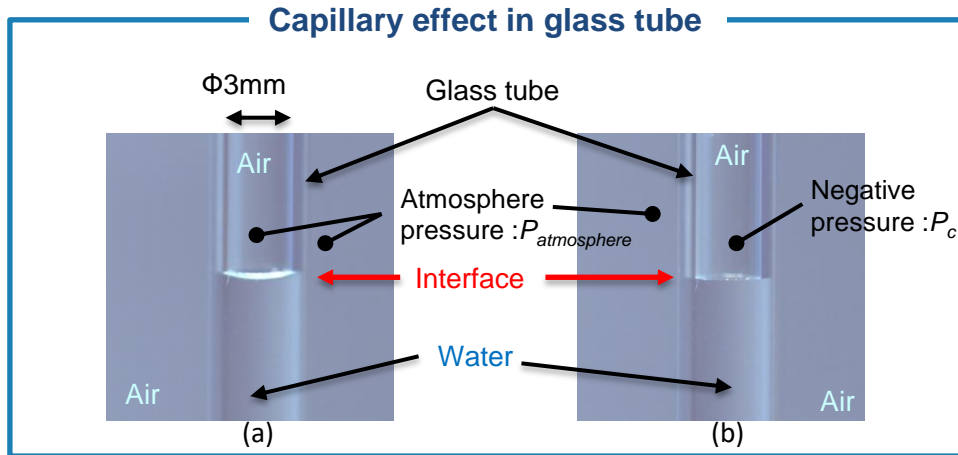


Fig. 2-7 Capillary effect of DIW in the glass tube of 3 mm diameter: (a) the border of water and air under the atmosphere pressure : $P_{atmosphere}$ and (b) the border of water and air under the negative pressure : P_c .

2-4. Conclusion

The minimum CD without pattern collapse was improved approximately 10% under the negative pressure during rinsing and drying processes. For 90 to 130 nm line patterns, 6 to 11% improvement was obtained, although no improvement was found for 60 and 45 nm line patterns. It is considered that the capillary force in photoresist patterns decreased because the contact angle between photoresist pattern and DIW increased. The negative pressure in this study was not enough large to mitigate pattern collapse of 45 and 60 nm line patterns.

References

- 1) T. Tanaka, M. Morigami, H. Oizumi, T. Soga, T. Ogawa, and F. Murai, J. Electrochemical Soc. **141**, 12 (1994).
- 2) H. Namatsu, K. Yamazaki, and K. Kurihara, Microelectronic Eng. **46**, 129 (1999).
- 3) K. Matsunaga, H. Oizumi, K. Kaneyama, G. Shiraishi, K. Matsumaro, J. J. Santillan, and T. Itani, Proc. SPIE **7636**, 76360S (2010).
- 4) T. S. Kulmala, M. Vockenhuber, E. Buitrago, R. Fallica, and Y. Ekinici, J. Micro/Nanolith. MEMS MOEMS **14**, 033507 (2015).
- 5) T. Tanaka, M. Morigami, and N. Atoda, J. Appl. Phys. **32**, 6059 (1993).
- 6) H. Namatsu, K. Kurihara, M. Nagase, K. Iwadate, and K. Murase, Appl. Phys. Lett. **66**, 2655 (1995).
- 7) M. Sanada, M. Sugiyama, M. Jaramillo Jr, P. Zhang, and S. Cassel, Proc. SPIE **6153**, 615331 (2006).
- 8) K. Yamamoto and T. Itani, Proc. SPIE **9422**, 94221Y (2015).
- 9) P. Zhang, M. B. Rao, M. Jaramillo, Jr., B. Horvath, B. Ross, T. Paxton, T. Davis, P. Cook, and D. Witko, Proc. SPIE **5753**, 252 (2005).

- 10) H. Namatsu, K. Yamazaki, and K. Kurihara, *J. Vac. Sci. Technol.* **B18**, 780 (2000).
- 11) A. E. Zweber, M. Wagner, J. D. Young, and R. G. Carbonell, *Langmuir* **25**, 6176 (2009).
- 12) Y. Kikuchi, T. Fukuda, and H. Yanazawa, *J. Photopolym. Sci. Technol.* **16**, 369 (2003).
- 13) T. Tanaka, M. Morigami, H. Oizumi, and T. Ogawa, *Jpn. J. Appl. Phys.* **32**, 5813 (1993).
- 14) W. Shibayama, S. Shigaki, M. Nakajima, S. Takeda, R. Onishi, and R. Sakamoto, *J. Photopolym. Sci. Technol.* **29**, 469 (2016).
- 15) D. G. Oteyza, P. N. Perera, M. Schmidt, M. Falch, S. D. Dhuey, B. D. Harteneck, A. M. Schwartzberg, P. J. Schuck, S. Cabrini, and D. L. Olynick, *Nanotechnology* **23**, 185301 (2012).
- 16) V. Auzelyte, A. Langner, and H. H. Solak, *J. Vac. Sci. Technol.* **B27**, 2990 (2009).
- 17) P. K. Kulshreshtha, K. Maruyama, S. Kiani, D. Ziegler, J. Blackwell, D. Olynick, and P. D. Ashby, *Proc. SPIE* **8681**, 86810O (2013).
- 18) G. Winroth, T. R. Younkin, J. M. Blackwell, and R. Gronheid, *J. Micro/Nanolith. MEMS MOEMS* **11**, 033004 (2012).
- 19) R. Sakamoto, B.-C. Ho, N. Fujitani, T. Endo, and R. Ohnishi, *Proc. SPIE* **7969**, 79692F (2011).
- 20) C. Y. Chang, D. C. Yu, J. H. Chen, J. C. H. Lin, B. J. Lin, J. W. Thackeray, V. Vohra, G. Wayton, and T. Kurihara, *Proc. SPIE* **6153**, 61530M (2006).
- 21) M. Harumoto, J. J. Santillan, C. Nakayama, Y. Tanaka, T. Motono, M. Asai, and T. Itani, *J. Photopolym. Sci. Technol.* **32**, 321 (2019).
- 22) H. Tsubaki, W. Nihashi, T. Tsuchihashi, T. Fujimori, M. Momota, and T. Goto, *J. Photopolym. Sci. Technol.* **28**, 489 (2015).
- 23) M. Harumoto, S. Negoro, A. Hisai, M. Tanaka, G. Mori, and M. Slezak, *Proc. SPIE* **7273**, 72730P (2009).
- 24) M. Harumoto, S. Suyama, T. Miyagi, A. Hisai, and M. Asai, *Proc. SPIE* **7639**, 763920 (2010).
- 25) M. Harumoto, O. Tamada, T. Miyagi, K. Kaneyama, A. Morita, C. Pieczulewski, and M. Asai, *Proc. SPIE* **8679**, 86792W (2013).
- 26) M. Harumoto, H. Stokes, O. Tamada, T. Miyagi, K. Kaneyama, C. Pieczulewski, and M. Asai, *Proc. SPIE* **9051**, 90510P (2014).
- 27) S. Harold, V. Jelle, D. Waut, M. Harumoto, and M. Asai, *Proc. SPIE* **10586**, 105860J (2018).
- 28) M. Harumoto, H. Stokes, Y. Thouroude, O. Tamada, T. Miyagi, K. Kaneyama, C. Pieczulewski, and M. Asai, *Proc. SPIE* **9048**, 904829 (2014).
- 29) D.C. Owe-Yang, T. Yano, T. Ueda, M. Iwabuchi, T. Ogihara, and S. Shirai, *Proc. SPIE* **6923**, 69232I (2008).
- 30) D. E. Noga, R. A. Lawson, C. -T. Lee, L. M. Tolbert, and C. L. Henderson, *Proc. SPIE* **7273**, 727334 (2009).
- 31) M. Sanada, O. Tamada, A. Ishikawa, and A. Kawai, *Proc. SPIE* **5753**, 988 (2005).
- 32) N. R. Tas, M. Escalante, J. W. Honschoten, H. V. Jansen, and M. Elwenspoek, *Langmuir* **26**, 1473 (2010).
- 33) K. Takahashi, T. Matsuo, M. Furuta, S. Oshima, K. Inaba, and K. Kishimoto, *J. Soc. Mechanical Eng.* **2**, 227 (2016).

34) T. Sanada, H. Nozaki, and M. Watanabe, J. Soc. Mechanical Engineers **82**, 838 (2016).

Chapter 3

Dependence of photoresist dissolution dynamics

in alkaline developers

on alkyl chain length of tetraalkylammonium hydroxide

3-1. Introduction

The resolution of photoresist materials used for semiconductor lithography has been improved and will continue to be improved to meet the market demands of highly integrated semiconductor devices.¹⁻⁷⁾ However, stochastic defects such as line bridges and breaks, which are randomly generated, become the new issues on sub-20-nm half-pitch patterns.⁸⁻¹⁵⁾ The cause of stochastic defects is assumed to be the small and insufficient number of photons delivered to the photoresist film (compared with that in ArF immersion)¹⁵⁻¹⁸⁾ or the effect of the molecular weight of the photoresist polymer.^{9,19-21)} On the basis of these pointers, photoresists continue to be improved to solve the stochastic defect problem.^{14-15,22-24)} Another factor considered as a possible solution is the developer solution utilized.²⁵⁻³²⁾ An aqueous solution of 0.26 N tetramethylammonium hydroxide (TMAH) has been used for many years as an alkaline developer of choice for the development process (in which a pattern formation of exposed photoresist occurs). Recent reports on EUV lithography have shown the application of new developer solutions such as tetrabutylammonium hydroxide (TBAH) to improve photoresist performance [e.g., the reduction in line width roughness (LWR)].³³⁻³⁷⁾

The quartz crystal microbalance (QCM) method is a well-known technique to observe photoresist dissolution dynamics during the development process.³⁸⁻⁴¹⁾ It has been widely used to observe the dissolution dynamics of new resist materials at each lithography generation: KrF, ArF, ArF immersion, and extreme ultraviolet (EUV) lithographies. By measuring the dissolution rates of photoresist films in both exposed (deprotected) and unexposed (protected) states, it is possible to obtain information on the photoresist sensitivity and photoresist solubility-insolubility contrast during development at a given development time.

In this study, we investigated the dissolution dynamics of EUV photoresists by the QCM method using four types of alkaline developer with different alkyl chain lengths, TMAH, tetraethylammonium hydroxide (TEAH), tetrapropylammonium hydroxide (TPAH), and TBAH, to clarify the swelling and dissolution kinetics of EUV resists. The backbone polymers of EUV resists used were poly(4-hydroxystyrene) (PHS), poly(methacrylic acid), and their copolymer.

3-2. Experimental

3-2-1. Materials

Figure 3-1 shows the three types of photoresist polymer utilized in the experiment: PHS, acryl, and a PHS-acryl hybrid. The polymer of the PHS-type photoresist was composed of PHS and 2-methoxyadamantane (AdMA)-protected PHS. For the acryl-type photoresist, the polymer was composed of γ -butyrolactone-2yl methacrylate (GBLMA), 2-methyl-2-adamantyl methacrylate (MAdMA), and 3-hydroxy-1-adamantylmethacrylate (HAdMA). For the PHS-acryl-hybrid-type photoresist, the polymer was composed of PHS and MAdMA. Triphenylsulfonium-trifluoromethanesulfonate (TPS-triflate) was used as a photoacid generator (PAG) and tri-n-octylamine (TOA) was used as a quencher for each photoresist. As mentioned earlier, four types of alkaline developer, TMAH, TEAH, TPAH, and TBAH aqueous solutions, were used, as shown in Fig. 3-2. The normality of solutions was adjusted to 0.26 N.

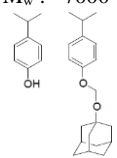
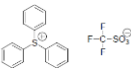
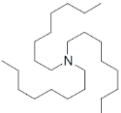
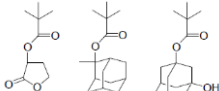
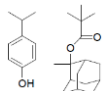
Name	Chemical structure			Solvent
	Polymer	PAG	Quencher	
PHS	PHS/AdMA(60/40) M_w : ~7000 	TPS-Triflate 	TOA 	PGMEA/PGME (60/40)
Acryl	GBLMA/MAdMA/HAdMA (45/35/20) M_w : ~11,000 	PHS : 4-hydroxystyrene AdMA : 2-adamantyl methacrylate MAdMA : 2-methyl-2-adamantyl methacrylate GBLMA : γ -butyrolactone-2yl methacrylate HAdMA : 3-hydroxy-1-adamantylmethacrylate TPS-Triflate : triphenylsulfonium-trifluoromethanesulfonate TOA : tri-n-octylamine		
Hybrid	PHS/MAdMA (60/40) M_w : ~7,000 			

Fig. 3-1 Photoresist polymers utilized in this study.

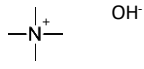
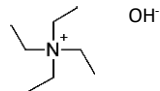
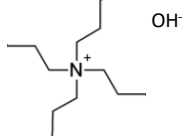
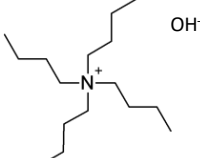
Developer name	Chemical structure
TMAH (Tetramethylammonium Hydroxide)	
TEAH (Tetraethylammonium Hydroxide)	
TPAH (Tetrapropylammonium Hydroxide)	
TBAH (Tetrabutylammonium Hydroxide)	

Fig. 3-2 Tetraalkylammonium hydroxide used in this study.

3-2-2. Measurement of photoresist contrast curve

The photoresists with a film thickness of 36 nm were coated on Si substrates and baked at 110°C for 60 s. A large-area (1 × 1 cm²) EUV exposure was performed, utilizing an in-house EUV frame exposure tool (Litho Tech Japan). The EUV source was EQ-10M (Energetiq Technology). After EUV exposure, the samples were baked (postexposure baking, PEB) at 100 °C for 60 s. The samples were developed in alkaline developers (as indicated in Fig. 3-2) for 30 s and rinsed with deionized water (DIW) for 30 s. Finally, the remaining film thickness of photoresists after development was measured using VM-3010 (SCREEN).

3-2-3. QCM measurement

The photoresist dissolution dynamics were measured by QCM, specifically by using the RDA-Qz3 (Litho Tech Japan). The photoresist films were coated on QCM substrates and baked at 110 °C for 60 s. The coated photoresists were irradiated with UV light with a wavelength of 254 nm (AS ONE Handy UV Lamp SLUV-6) and then baked at 100°C for 60 s. It is known that PAG reacts with secondary electrons generated upon exposure to EUV radiation.^{13,18,42,43} However, the wavelength of 254 nm was used to generate acids in this study, because the purpose of this study is to clarify the dissolution

dynamics of EUV resists. A high reproducibility of experimental data is expected by using 254 nm UV light. The photoresists were developed with each alkaline developer (Fig. 3-2) at 23°C and rinsed with DIW in the QCM tool. The film thicknesses of the photoresist on the QCM substrates after coating and developing were measured using an ellipsometer FS-1 (Meiwafosis).

QCM measurement can detect extremely small mass changes on the order of nanograms from the resonant frequency of quartz crystal in situ during development. It is known that the relationship between the frequency change Δf and the mass change Δm in QCM measurement is expressed as

$$\Delta f = -\frac{2f_0^2}{A\sqrt{\rho_q\mu_q}}\Delta m, \quad (1)$$

where f_0 is the resonant frequency, A is the gold electrode area on the quartz substrate, ρ_q is the density of quartz crystal, and μ_q is the shear modulus.⁴⁴⁾ Note that this equation is valid under the condition that the material observed on the substrate is rigid. However, the transient swelling layer is not rigid, which we should take into consideration.

3-3. Results and discussion

3-3-1. Photoresist contrast curves

Photoresist contrast curves were measured to roughly overview the response of photoresists to EUV radiation and the type of developer. Figure 3-3 shows the photoresist contrast curves for the PHS-type, acryl-type, and hybrid-type photoresists developed in the various alkaline developers considered after being irradiated with 13.5-nm-wavelength light and baked at 100 °C for 60 s. The vertical axis represents the relative film thickness after development. The film thickness before exposure was set to 1 in each graph. The horizontal axis represents exposure dose. The blue, red, orange, and purple curves represent the cases of photoresists developed in 0.26 N TMAH, 0.26 N TEAH, 0.26 N TPAH, and 0.26 N TBAH aqueous solutions, respectively. The ranges of E_{th} , that is, the exposure energy thresholds at which the photoresist film was completely dissolved after the development process, were 0.7-1.0 mJ/cm² for the PHS-type photoresist, 1.0-1.4 mJ/cm² for the acryl-type photoresist, and 1.1-1.5 mJ/cm² for the hybrid-type photoresist. The E_{th} of the PHS-type photoresist with the TMAH developer was smaller than those of the acryl-type and hybrid-type photoresists with the TMAH developer. In this study, the difference in E_{th} among the photoresist types is not discussed, because the quantum yield of acids (acid generation efficiency) depends on the type of photoresist polymer. We cannot distinguish

between two effects (the acid quantum yield and the developer). Therefore, the effects of alkaline aqueous developers are compared for each type of photoresist. Then, the trends of the effects of alkaline aqueous developers are discussed for all the photoresists used in this study. The E_{th} of the PHS-type photoresist was smaller than those of the acryl-type and hybrid-type photoresists for all the alkaline developers used. For the PHS-type and acryl-type photoresists, the use of a high-molecular-weight alkaline developer tended to result in a large E_{th} (or required a high exposure dose to dissolve completely). In the case of the hybrid-type photoresist, the use of a high-molecular-weight alkaline developer decreased E_{th} . The details of dissolution dynamics are hereafter discussed on the basis of QCM charts.

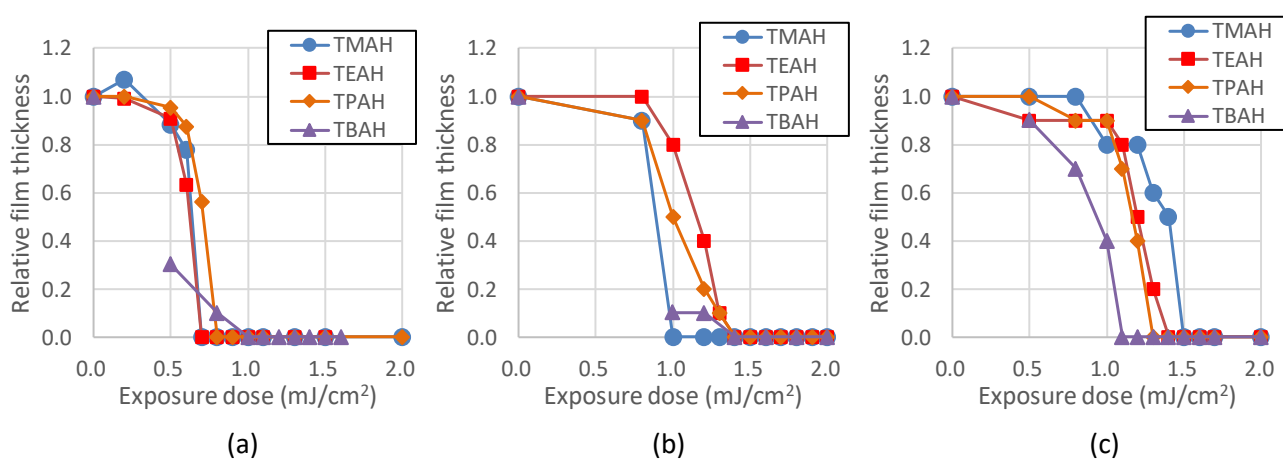


Fig. 3-3 Photoresist contrast curves for (a) PHS-type, (b) acryl-type, and (c) hybrid-type photoresists developed in alkaline developers after being exposed to EUV radiation with wavelength of 13.5 nm and baked at 100 °C for 60 s.

3-3-2. Dissolution dynamics of PHS-type photoresist

PHS molecules are soluble in the 0.26 N alkaline developer. In the 0.26 N alkaline developer, the hydroxyl groups of PHS dissociate (are ionized). Subsequently, the PHS molecules are hydrated, dissolved and transported to the bulk solution. The PHS-type photoresist utilized PHS molecules, of which 40 mol% of the hydroxyl groups are protected by nonpolar groups. Therefore, polar and nonpolar interactions occur between PHS-type photoresist polymers. Owing to the nonpolar interaction, the PHS photoresist is insoluble in the 0.26 N alkaline developer. The acids generated upon exposure to UV deprotect the nonpolar groups and change them to hydroxyl groups. Figure 3-4 shows the QCM charts of the PHS-type photoresist during development after being exposed to UV light with a wavelength of 254 nm. Upon the immersion of the QCM substrate into the developer, the frequency

decreased by approximately 700–800 Hz owing to the viscosity of the developer. The frequency immediately after immersion was set to 0 (base value). The QCM charts in Figs. 3-4(a) and 3-4(d) were obtained in the TMAH, TEAH, TPAH, and TBAH developers, respectively. The frequency changes (vertical axis) represent the mass changes of the exposed PHS photoresist film (coated on the QCM substrate) during development. According to Eq. (1), the positive direction of the vertical axis indicates a decrease in the mass of the photoresist on the QCM substrate, that is, the dissolution of the photoresist film. On the other hand, the negative direction indicates an increase in the mass of the photoresist, that is, the swelling caused by the penetration of the developer into the photoresist film.^{41,45,46} As shown in Fig. 3-4, the frequencies were approximately constant at the exposure dose of 0 mJ/cm². The water did not penetrate into the resist films owing to a strong nonpolar interaction. A slight decrease in frequency was observed at 4 mJ/cm². The developer penetrated into PHS photoresists as a result of deprotection (the increase in OH group density). However, the reduction in film thickness was not observed. Although water was absorbed, it was insufficient to break the nonpolar interaction between resist polymers. At 6 mJ/cm², the dissolution of photoresist films was observed. The dissolution rate of photoresist films increased with exposure dose in all the developers. The PHS-type photoresist film exposed to 10 mJ/cm² UV light was completely dissolved, while that exposed to 6.5 mJ/cm² UV light was approximately half-dissolved after 60 s development. For all the developers, a similar trend of dissolution was observed. The dissolution dynamics of the PHS-type photoresist did not depend on the alkyl chain length of tetraalkylammonium hydroxide. This suggests that the dissociation of the resist polymer was not affected by the alkyl chain length of tetraalkylammonium hydroxide. The alkyl chain length of tetraalkylammonium cations was also considered to not affect the penetration of tetraalkylammonium cations into the PHS-type photoresist films.

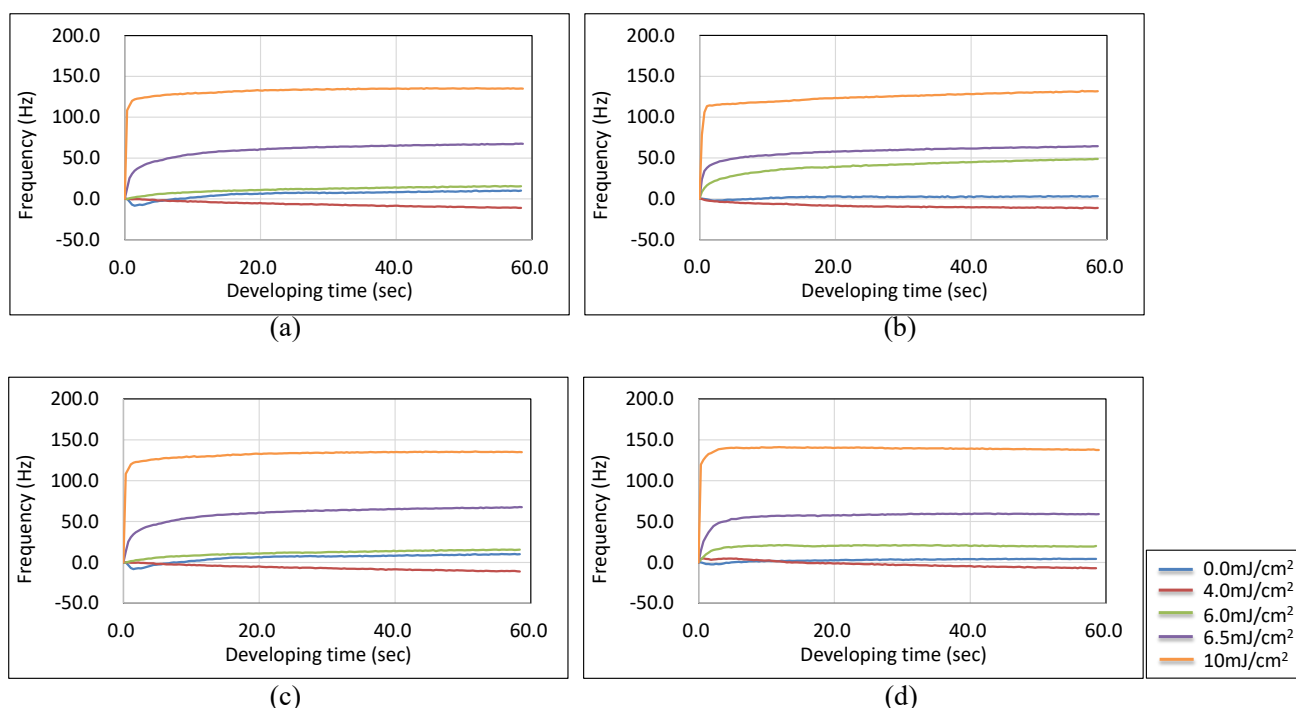


Fig. 3-4 QCM charts of PHS-type photoresist during development in (a) TMAH, (b) TEAH, (c) TPAH, and (d) TBAH developers. Numerical values in mJ/cm^2 are UV exposure doses.

3-3-3. Dissolution dynamics of acryl-type photoresist

Figure 3-5 shows the QCM charts of the acryl-type photoresist during development in the TMAH, TEAH, TPAH, and TBAH developers. The dissolution dynamics of the acryl-type photoresist was significantly different from that of the PHS-type photoresist and depended on the alkyl chain length of tetraalkylammonium hydroxide. In the acryl-type photoresist, the dissolution agent is carboxylic acid unlike the PHS-type photoresist. The acryl-type photoresist utilized poly(methacrylic acid), of which all carboxylic acid groups are protected by nondissociative units. Among the protected units, MAdMA units are deprotected by acid catalytic reaction and converted to carboxylic acids. In 0.26 N alkaline, the carboxylic acids dissociate. Subsequently, the resist molecules are hydrated, dissolved, and transported. The pK_a of carboxylic acids is lower than that of phenolic hydroxyl groups. HAdMA units have an alcoholic hydroxyl group. Although the alcoholic hydroxyl group is not dissociated in an alkaline developer (that is, the contribution to the polymer dissolution is small, unlike the phenolic hydroxyl group), it promotes water intake. The GBLMA units were incorporated for adhesion control. At an exposure dose of $0 \text{ mJ}/\text{cm}^2$ UV, swelling was not observed. At an exposure dose of $11 \text{ mJ}/\text{cm}^2$ UV, significant swelling was observed for TMAH. The alcoholic hydroxyl groups are probably one cause

of this swelling because they contribute to water intake and do not contribute to dissociation. The swelling rate decreased with increasing alkyl chain length of tetraalkylammonium hydroxide. For TBAH, the swelling was mostly suppressed. As observed in the PHS-type photoresist, the alkyl chain length of tetraalkylammonium cations is unlikely to affect the dissociation of the resist polymer. For the acryl-type photoresist, the alkyl chain length of tetraalkylammonium cations is considered to significantly affect the penetration of tetraalkylammonium cations into the photoresist films. Above the exposure dose of 13 mJ/cm², the acryl-type photoresist dissolved with the formation of a thick transient swelling layer. In such a case, the alkyl chain length of tetraalkylammonium cations affected the formation of the transient swelling layer.

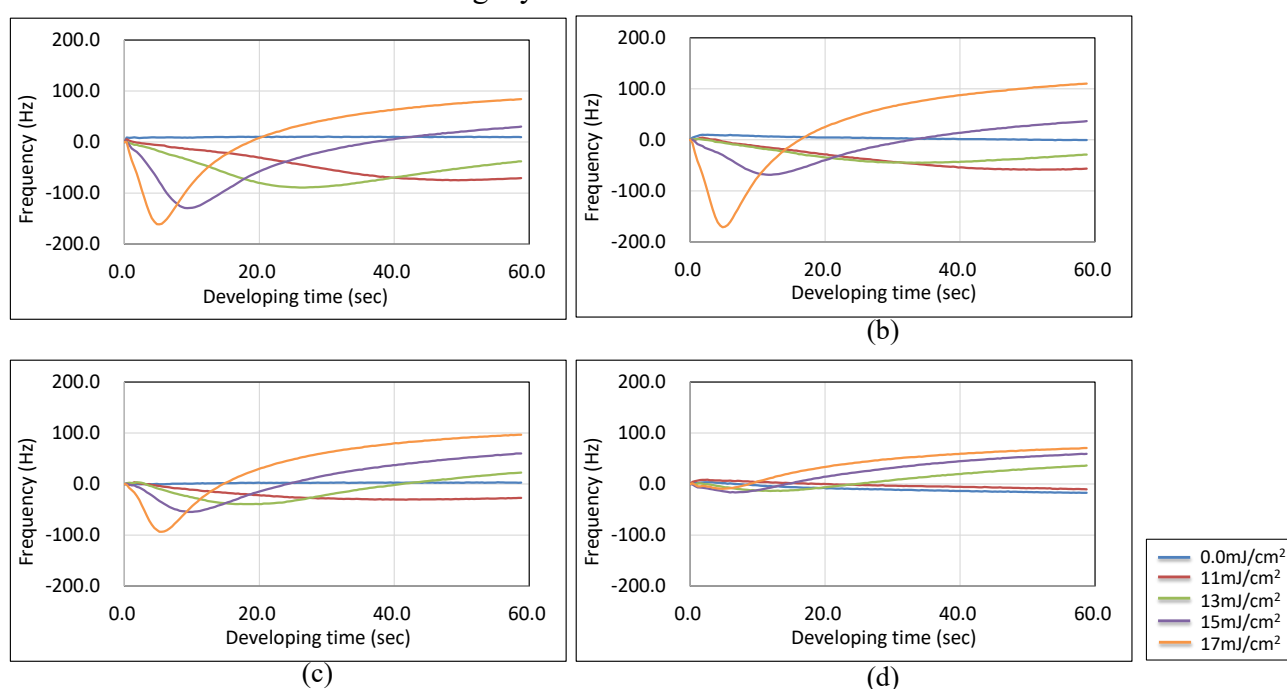


Fig. 3-5 QCM charts of acryl-type photoresist during development in (a) TMAH, (b) TEAH, (c) TPAH, and (d) TBAH developers. Numerical values in mJ/cm² are UV exposure doses.

3-3-4 Dissolution dynamics of hybrid-type photoresist

Figure 3-6 shows the QCM charts of the hybrid-type photoresist during development in the TMAH, TEAH, TPAH, and TBAH developers. A similar trend to the PHS-type resist was observed. However, the dissolution rate increased with the alkyl chain length of tetraalkylammonium cations. In the hybrid-type photoresist, the dissolution agents are carboxylic acids and phenolic hydroxyl groups. In the hybrid-type photoresist, the methacrylic acid units are generally protected by nonpolar groups. This is because the change in solubility upon deprotection for the acryl units is larger than that for PHS units

because of the difference in pK_a . The acryl units are deprotected by acid catalytic reaction and converted to carboxylic acids. In 0.26N alkaline, the carboxylic acids and phenolic hydroxyl groups dissociated. Subsequently, the resist molecules were hydrated and dissolved. At exposure doses of 0.0 and 8.0 mJ/cm^2 , the dissolution dynamics were approximately the same among the alkaline developers within experimental error. The alkyl chain length did not significantly affect the penetration of water and tetraammonium cations into the photoresist films. Above the exposure dose of 12 mJ/cm^2 , the dissolution rate tended to increase with the alkyl chain length of tetraalkylammonium cations. This corresponded to the dependence of E_{th} shown in Fig. 3-3(c). The long alkyl chain is considered to be effective in breaking the hydrophobic interaction between resist polymers in the case of the hybrid-type photoresist.

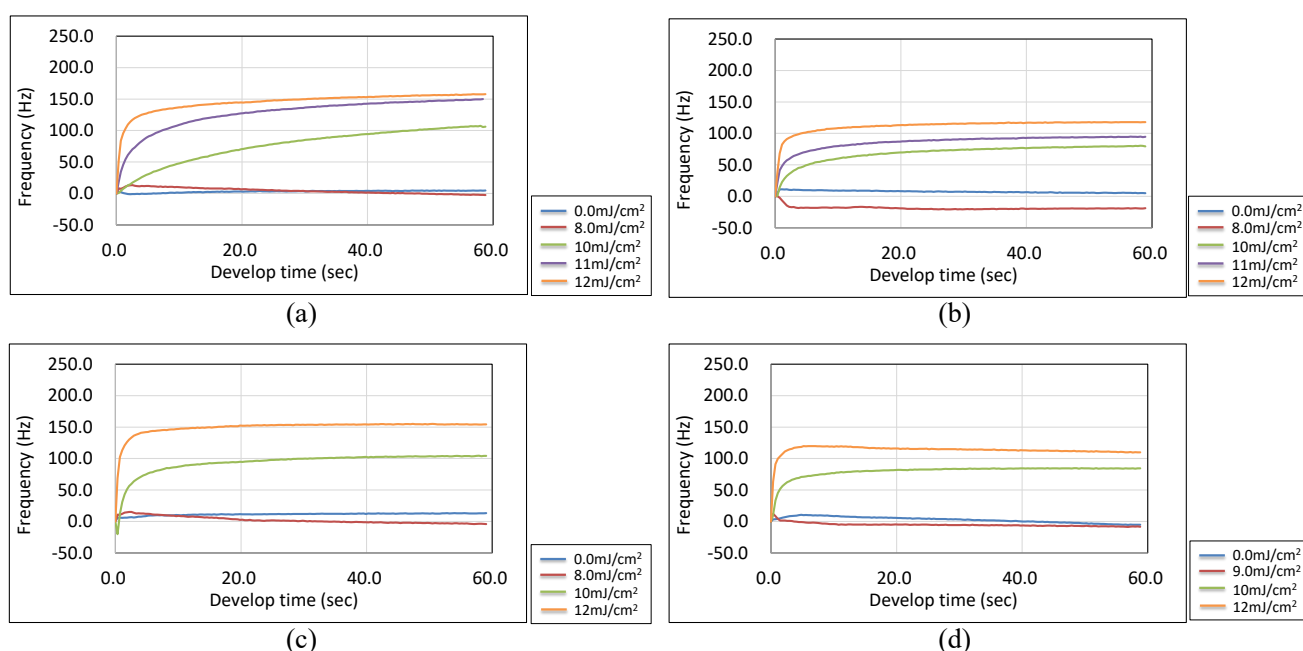


Fig. 3-6 QCM charts of hybrid-type photoresist during development in (a) TMAH, (b) TEAH, (c) TPAH, and (d) TBAH developers. Numerical values in mJ/cm^2 are UV exposure doses.

3-4. Conclusion

The dissolution dynamics of EUV photoresists were investigated by the QCM method using four types of alkaline developer with different alkyl chain lengths: TMAH, TEAH, TPAH, and TBAH. There were no significant differences in dissolution dynamics between alkaline developers for the PHS-type photoresist. However, large differences were observed for the acryl-type photoresist. Moreover, for the acryl-type photoresist, the small tetraalkylammonium cation caused much swelling during the initial

stage of the development process. It is considered that the small cation easily penetrates into the acryl polymer. For the hybrid-type photoresist, however, the dissolution rate increased with the alkyl chain length of tetraalkylammonium cations. The long alkyl chain is considered to be effective in breaking the hydrophobic interaction between resist polymers in the case of the hybrid-type photoresist.

References

- 1) X. Chen, A. Gabor, P. Samudrala, S. Meyers, E. Hosler, R. Johnson, and N. Felix, Proc. SPIE **10143**, 10143F (2017).
- 2) R. van Es, M. van de Kerkhof, A. Minnaert, G. Fisser, J. de Klerk, J. Smits, R. Moors, E. Verhoeven, L. Levasier, R. Peeters, M. Pieters, and H. Meiling, Proc. SPIE **10583**, 105830H (2018).
- 3) T. Song, J. Jung, W. Rim, H. Kim, Y. Kim, C. Park, J. Do, S. Park, S. Cho, H. Jung, B. Kwon, H. S. Choi, J. S. Choi, and J. S. Yoon, ISSCC **11.2**, 198-200 (2018).
- 4) G. Yeap, S. S. Lin, Y. M. Chen, S. M. Jang et al., IEEE IEDM **879**, 3671 (2019).
- 5) S. M. Y. Sherazi, M. Cupak, P. Weckx, O. Zografos, D. Jang, P. Debacker, D. Verkest, A. Mocuta, R. H. Kim, A. Spessot, and J. Ryckaert, Proc. SPIE **10962**, 1096202 (2019).
- 6) T. Y. Jeong, M. Lee, Y. Jo, J. Kim, M. Kim, M. Yeo, J. Kim, H. Choi, J. Kim, Y. Jo, Y. Ji, T. Uemura, H. Jiang, D. Kwon, H. S. Rhee, S. Pae, and B. Lee, IEEE IRPS **459451**, 19733275 (2020).
- 7) T. Y. J. Chang, Y. H. Chen, W. M. Chan, H. Cheng, P. S. Wang, Y. Lin, H. Fujiwara, R. Lee, H. J. Liao, P. W. Wang, G. Yeap, and Q. Li, IEEE J. Solid-state Circuits **56**, 179 (2021).
- 8) W. Gao, A. Philippou, U. Klostermann, J. Siebert, V. Philipsen, E. Hendrickx, T. Vandeweyer, and G. Lorusso, Proc. SPIE **8322**, 83221D (2012).
- 9) T. Kozawa, J. J. Santillan, and T. Itani, Jpn. J. Appl. Phys. **52**, 076502 (2013).
- 10) P. D. Bisschop, J. V. Kerkhove, J. Mailfert, A. V. Pret, and J. Biafore, Proc. SPIE **9048**, 904809 (2014).
- 11) A. V. Pret, P. D. Bisschop, M. D. Smith, and J. Biafore, Proc. SPIE **9048**, 904834 (2014).
- 12) P. D. Bisschop and E. Hendrickx, Proc. SPIE **10583**, 105831K (2018).
- 13) T. Kozawa, J. J. Santillan, and T. Itani, J. Photopolym. Sci. Technol. **32**, 161 (2019).
- 14) P. D. Bisschop and E. Hendrickx, Proc. SPIE **10957**, 109570E (2019).
- 15) K. Nishikori, K. Kasahara, T. Kaneko, T. Sakurai, S. Dei, K. Maruyama, and R. Ayothi, Proc. SPIE **11326**, 1132612 (2020).
- 16) R. L. Brainard, P. Trefonas, J. H. Lammers, C. A. Cutler, J. F. Mackevich, A. Trefonas, and S. A. Robertson, Proc. SPIE **5374**, 74 (2004).
- 17) J. J. Biafore, M. D. Smith, C. A. Mack, J. W. Thackeray, R. Gronheid, S. A. Roberson, T. Graves, and D. Blankenship, Proc. SPIE **7273**, 727343 (2009).
- 18) S. Fujii, T. Kozawa, K. Okamoto, J. J. Santillan, and T. Itani, J. Appl. Phys. **54**, 086502 (2015).
- 19) T. Kozawa, J. J. Santillan, and T. Itani, J. Appl. Phys. **53**, 084002 (2014).
- 20) T. Kozawa, J. Appl. Phys. **54**, 016502 (2015).
- 21) A. Nakajima, M. Hoshino, M. Hashimoto, and T. Kozawa, J. Appl. Phys. **58**, 020909 (2019).

- 22) H. Furutani, M. Shirakawa, W. Nihashi, K. Sakita, H. Oka, M. Fujita, T. Omatsu, T. Tsuchihashi, N. Fujimaki, and T. Fujimori, *J. Photopolym. Sci. Technol.* **31**, 201 (2018).
- 23) A. D. Silva, L. Meli, D. L. Goldfarb, and N. M. Felix, *Proc. SPIE* **10957**, 109570F (2019).
- 24) A. Shirotori, M. Hoshino, D. D. Simone, G. Vandenberghe, and H. Matsumoto, *Proc. SPIE* **11517**, 115170D (2020).
- 25) O. Tamada and M. Sanada, *Proc. SPIE* **5753**, 996 (2005).
- 26) C. Y. Chang, D. C. Yu, J. H. Chen, J. C. H. Lin, and B. J. Lin, *Proc. SPIE* **6153**, 61530M (2006).
- 27) Y. Wei, K. Petrillo, S. Brandl, F. Goodwin, P. Benson, R. Housley, and U. Okoroanyanwu, *Proc. SPIE* **6153**, 615306 (2006).
- 28) O. Miyahara, T. Shimoaoki, R. Naito, K. Yoshihara, and J. Kitano, *Proc. SPIE* **6153**, 61533K (2006).
- 29) V. Huang, C. C. Chiu, C. A. Lin, C. Y. Chang, T. S. Gau, and B. J. Lin, *Proc. SPIE* **6519**, 65193C (2007).
- 30) M. Harumoto, A. Yamaguchi, and A. Hisai, *Proc. SPIE* **6519**, 65193F (2007).
- 31) M. Harumoto, T. Kuroda, M. Sugiyama, and A. Hisai, *Proc. SPIE* **6923**, 69233J (2008).
- 32) M. Harumoto, S. Negoro, A. Hisai, M. Tanaka, G. Mori, and M. Slezak, *Proc. SPIE* **7273**, 72730P (2009).
- 33) T. Itani and J. J. Santillan, *J. Vac. Sci. Technol. B* **27**, 2986 (2009).
- 34) K. Matsunaga, H. Oizumi, K. Kaneyama, G. Shiraishi, K. Matsumaro, J. J. Santillan, and T. Itani, *Proc. SPIE* **7636**, 76360S (2010).
- 35) M. Harumoto, K. Shigemori, A. Hisai, M. Asai, and K. Kaneyama, *Proc. SPIE* **7636**, 76362Z (2010).
- 36) K. Kaneyama, K. Matsunaga, G. Shiraishi, J. J. Santillan, and T. Itani, *Proc. SPIE* **7636**, 763633 (2010).
- 37) J. J. Santillan, M. Harumoto, H. Stokes, C. Mori, Y. Tanaka, Y. Arisawa, T. Motono, M. Asai, and T. Itani, *Proc. SPIE* **11323**, 113231W (2020).
- 38) M. Toriumi, *Proc. SPIE* **5753**, 302 (2005).
- 39) M. Toriumi, *Proc. SPIE* **7273**, 72732Y (2009).
- 40) A. Sekiguchi, *J. Photopolym. Sci. Technol.* **23**, 421 (2010).
- 41) A. Konda, H. Yamamoto, S. Yoshitake, and T. Kozawa, *Proc. SPIE* **9776**, 977629 (2016).
- 42) T. Kozawa, Y. Yoshida, M. Uesaka, and S. Tagawa, *J. Appl. Phys.* **31**, 4301 (1992).
- 43) J. F. Cameron, N. Chan, K. Moore, and G. Pohlars, *J. Photopolym. Sci. Technol.* **14**, 345 (2001).
- 44) G. Sauerbrey, *Z. Phys.* **155**, 206 (1959).
- 45) A. Nakajima, K. Watanabe, K. Matsuoka, T. Kozawa, Y. Komuro, D. Kawana, and A. Yamazaki, *Jpn. J. Appl. Phys.* **59**, 036505 (2020).
- 46) A. Nakajima, K. Matsuoka, and T. Kozawa, *Appl. Phys. Express* **14**, 206501 (2021).

Chapter 4

**Stochastic defect generation depending
on tetraalkylhydroxide aqueous developers
in extreme ultraviolet lithography**

4-1. Introduction

The patterning performance of photoresist materials continues to advance, meeting the demands of leading-edge semiconductor manufacturing technologies, namely, extreme ultraviolet lithography (EUVL).¹⁻⁵⁾ Even as first-generation EUVL is now being utilized for high-volume semiconductor manufacturing,^{1,6)} the industry is already starting to prepare for next-generation or high-numerical-aperture (high-NA) EUVL.⁷⁻¹⁰⁾ However, patterning targets for these leading-edge technologies (especially high-NA EUVL) are starting to push present photoresist materials [e.g., chemical amplification resists (CARs)] to their physical limits.²⁻⁵⁾ Besides pattern resolution, which has traditionally been the main performance metric for photoresists, the appearance of randomly occurring (stochastic) photoresist-based pattern defects is one of the main concerns and has become a constant topic of discussion in addition to line edge roughness (LER).¹¹⁻¹⁴⁾ LER has been reported to be mainly caused by insufficient number of EUV photons delivered to the photoresist film during EUV exposure (at least compared with previous lithographic technologies such as ArF immersion).¹⁵⁻¹⁷⁾ The root cause of stochastic defects is also the insufficient number of photons. However, the contribution of process and material factors to stochastic defect generation is different from that to LER.¹⁸⁻²²⁾ Focusing on CAR materials, when the number of photons delivered to the photoresist is insufficient, the amount of acids generated is also insufficient and causes non-uniformity in the reactions required for acid generation. This non-uniformity becomes more apparent during the chemical amplification process when the photoresist is baked. Eventually, such uniformities will result in randomly formed and unformed patterns after development. This emphasizes the significant role of the development process in the physical formation of stochastic defects, which underlies the consistent and continuous interest in the research of developer solutions.²³⁻³³⁾

In our previous study, also focusing on the effect of developer solutions on photoresist dissolution, we utilized three typical EUV photoresist materials [poly(4-hydroxystyrene) (PHS) type, acryl type, and a hybrid of PHS and acryl types]³⁴⁾ and investigated the effect of developer solutions on the dissolution characteristics of these photoresists using various alkyl chain lengths of tetraalkylammonium hydroxides [tetramethylammonium hydroxide (TMAH), tetraethylammonium hydroxide (TEAH), tetrapropylammonium hydroxide (TPAH), and tetrabutylammonium hydroxide (TBAH)]. Results showed that the dissolution behaviors of EUV photoresists depended on the

developer solutions. However, it is noteworthy that for a certain photoresist type (i.e., acryl type), large photoresist film swelling occurs during photoresist development with the small-alkyl-chain-length developer solution (i.e., TMAH).

In this work, EUV patterning experiments were carried out to understand the effect or impact of developer solution on stochastic defect generation in terms of the alkyl chain length of tetraalkylammonium hydroxide. To this end, we compared the contact hole (CH) patterning performance of the above-mentioned typical EUV photoresists processed in the developers with different alkyl chain lengths.

4-2. Experimental conditions

4-2-1. Materials

Figure 4-1 shows the photoresist polymers (PHS, acryl, and hybrid) and alkaline aqueous developer solutions (TMAH, TEAH, TPAH, and TBAH at 0.26 N) utilized in the experiment. The polymer of PHS-type photoresist was composed of the PHS and 2-methoxyadamantane (AdMA)-protected PHS. For the acryl-type photoresist, the polymer was composed of γ -butyrolactone-2-yl methacrylate (GBLMA), 2-methyl-2-adamantyl methacrylate (MAdMA), and 3-hydroxy-1-adamantylmethacrylate (HAdMA). For the hybrid-type photoresist, the polymer was composed of PHS and MAdMA. Triphenylsulfonium trifluoromethanesulfonate (TPS triflate) was used as a photoacid generator (PAG) and tri-*n*-octylamine (TOA) was used as a quencher for each photoresist.

Photoresist	Polymer	PAG	Quencher	Solvent	Developer	
PHS		 TPS-Triflate	 TOA	PGMEA/ PGME	TMAH	
	TEAH					
Acryl					PHS/MAAdMA	TBAH
	Hybrid		TBAH			

Fig. 4-1 (a) Photoresist polymers (PHS, acryl, and hybrid types) and (b) developer solutions (TMAH, TEAH, TPAH, and TBAH) utilized in the experiment.

4-2-2. Patterning experiments

A bilayer stack was formed on a Si substrate by spin coating. The underlayer was an organic film of 20 nm thickness. The underlayer was baked at 205 °C for 60 s after spin coating. The EUV photoresist (as indicated in the previous section), utilized as the top layer of 36 nm film thickness, was coated on the underlayer and baked at 110 °C for 60 s.

Photoresist processes (coating, baking, etc.) were performed in a coater/developer system, SOKUDO DUO coater/developer (SCREEN Semiconductor Solutions). EUV patterning was carried out using NXE:3400B (ASML), with 0.33 NA.^{1,35)}

A total of 101 dies were exposed to EUV on a 300-mm- ϕ wafer (die size: $x=26$ mm and $y=18$ mm) at the best fixed focus and a dose set from 20 to 121 mJ/cm² in steps of 1 mJ/cm². After EUV exposure, the investigated developer solutions were utilized and the substrate was rinsed with deionized water (DIW). Scanning electron microscopy (SEM) measurements were performed using CG5000 (Hitachi High-Technologies). The critical dimensions (CDs) of the target patterns were measured for use in photoresist stochastic defect evaluation.

4-2-3. Stochastic defect measurement

In these experiments, stochastic defect analysis was carried out utilizing the 42-nm- ϕ (70 nm pitch) CH patterns, and 1805 holes were sampled for each exposure dose condition, focusing on two main types of CH-related defect; closed CH and open CH (Fig. 4-2). These defects were determined by processing SEM images (taken at 100 K magnification with five images per exposure dose

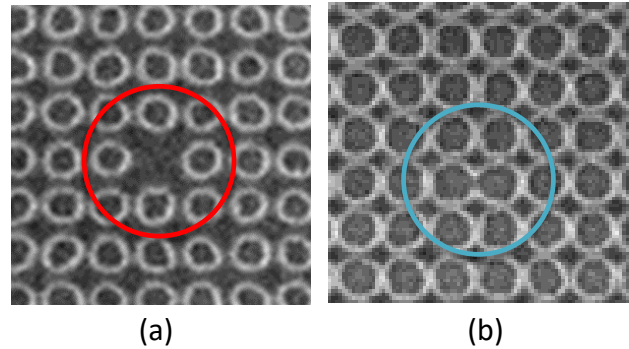


Fig. 4-2 Two types of CH-related defect: (a) closed and (b) open CH defects.

condition), using offline visual analysis. Classified CH defects were then tabulated and summarized with respect to CH CD to obtain the “*failure free CD-window*”³⁶⁾, which indicates the specific CH diameter region in the exposure dose range where no CH defects formed.

4-3. Results and discussion

4-3-1. Trend analysis of stochastic defects and *failure free CD-window*

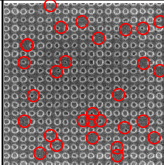
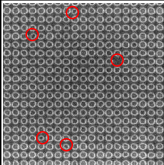
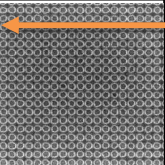
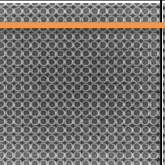
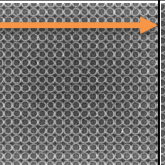
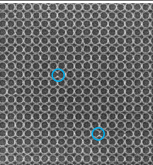
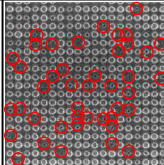
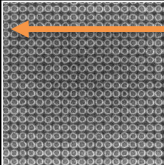
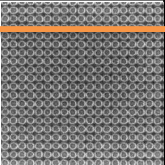
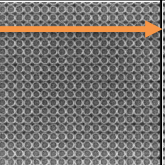
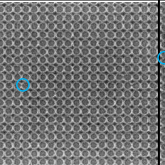
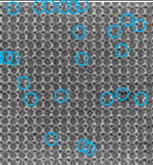
The CH patterns with 42-nm- ϕ (70 nm pitch) were fabricated by EUV exposure of PHS-, acryl-, and hybrid-type photoresists. Figure 4-3 shows the representative SEM images of CH patterns after being processed in TMAH and TBAH developers. Here, the SEM images show the patterning results at various exposure doses, where closed CH defects are indicated by red circles and open CH defects are indicated by blue circles. Orange arrows indicate the *failure free CD-window*.

At a low exposure dose, the CH diameter decreased, which in effect increased the occurrence of closed CH defects. On the other hand, at a high exposure dose, the CH diameter increased, which in effect increased the number of open CH defects. From these results, it is noteworthy that, in the case of the acryl-based photoresist developed in the TMAH developer, both closed and open CH defects coexisted at certain exposure doses (23 and 24 mJ/cm²).

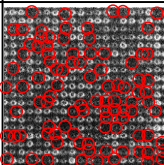
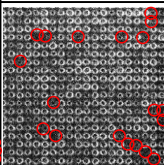
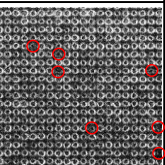
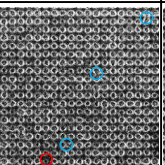
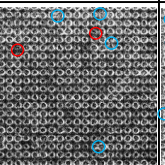
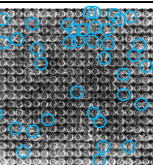
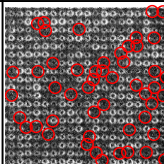
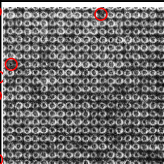
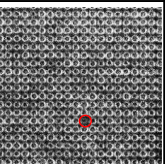
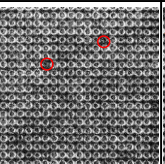
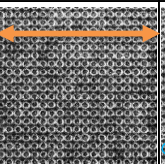
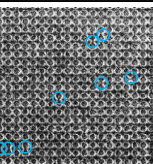
Figure 4-4 shows the number of closed and open CH defects depending on the measured CH diameters for PHS-, acryl-, and hybrid-type photoresists formed in TMAH, TEAH, TPAH, and TBAH developer solutions. These graphs also indicate the *failure free CD-window* (orange arrows), as mentioned in the previous section. From these raw data, the CH defect probability was calculated as

the percentage of defects with respect to the total of 1805 analyzed CHs for each exposure dose (i.e., “pattern failure ratios”). Figure 4-5 shows the *failure free CD-window* at various pattern failure ratios for PHS-, acryl-, and hybrid-type photoresists formed in TMAH, TEAH, TPAH, and TBAH developer solutions.

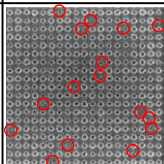
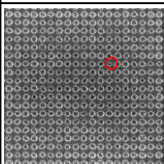
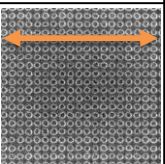
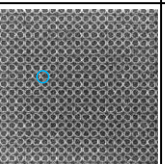
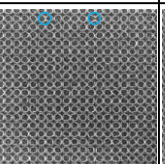
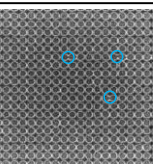
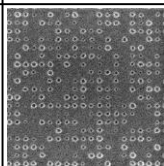
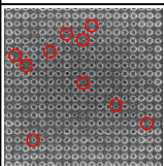
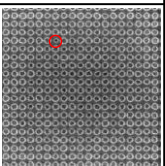
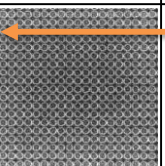
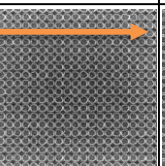
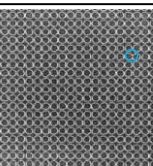
From these results, it was found that in the case of the PHS-type photoresist, the *failure free CD-window* was not significantly affected (almost the same value) by the alkyl chain length of tetraalkylammonium hydroxide in the low-pattern-failure-ratio region (<0.5%). In the case of the acryl-type photoresist, it was observed that the number of stochastic defects increased with the decrease in alkyl chain length. This resulted in a small *failure free CD-window*. A trend similar to that for the acryl-type photoresist was observed in the hybrid-type photoresist. The *failure free CD-window* for the hybrid-type photoresist was larger than that for the acryl-type photoresist.

Developer type	Exposure dose (mJ/cm ²)					
	40	43	45	50	51	53
TMAH						
	CHΦ (nm): 31.8	38.7	41.7	48.9	49.3	51.07
TBAH						
	CHΦ (nm): 30.8	40.1	43.0	50.5	51.0	--

(a)

Developer type	Exposure dose (mJ/cm ²)					
	20	21	22	23	24	25
TMAH						
	CHΦ (nm): 22.8	31.8	33.3	38.2	34.5	41.0
TBAH						
	CHΦ (nm): 24.7	34.6	37.3	38.8	40.9	--

(b)

Developer type	Exposure dose (mJ/cm ²)					
	48	49	55	67	69	70
TMAH						
	CHΦ (nm): 27.2	33.1	34.9	45.6	46.7	47.3
TBAH						
	CHΦ (nm): --	31.1	36.9	45.1	47.6	48.1

(c)

Fig. 4-3 Representative SEM images of 42-nm- ϕ (70-nm-pitch) CH patterns after EUV exposure for (a) PHS-, (b) acryl-, and (c) hybrid-type photoresists formed in TMAH and TBAH developers. SEM images show the patterning results at various exposure doses where closed CH defects are indicated by red circles and open CH defects are indicated by blue circles. An orange arrow indicates the *failure free CD-window*.

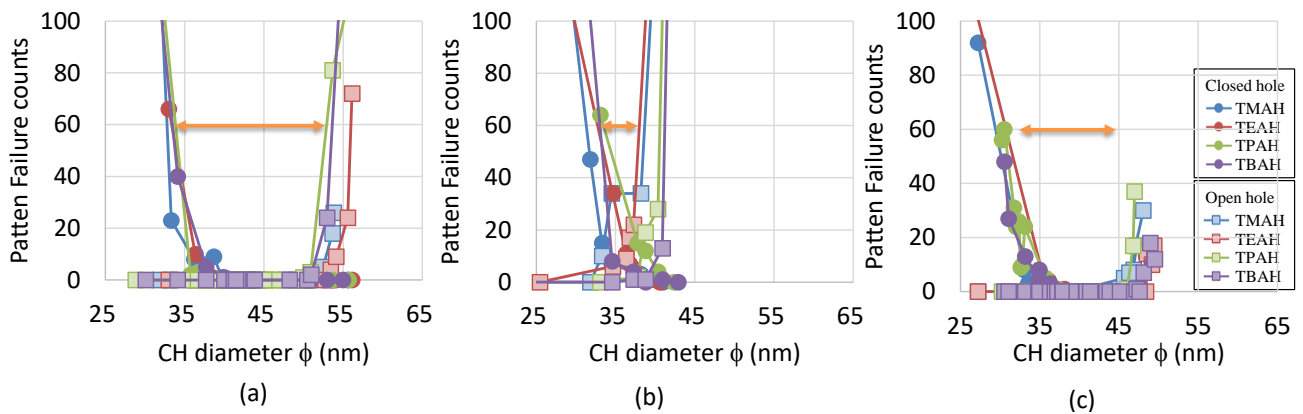


Fig. 4-4 The number of closed and open CH defects depending on the measured CH diameters for (a) PHS-, (b) acryl-, and (c) hybrid-type photoresists in various developer solutions (TMAH, TEAH, TPAH, and TBAH).

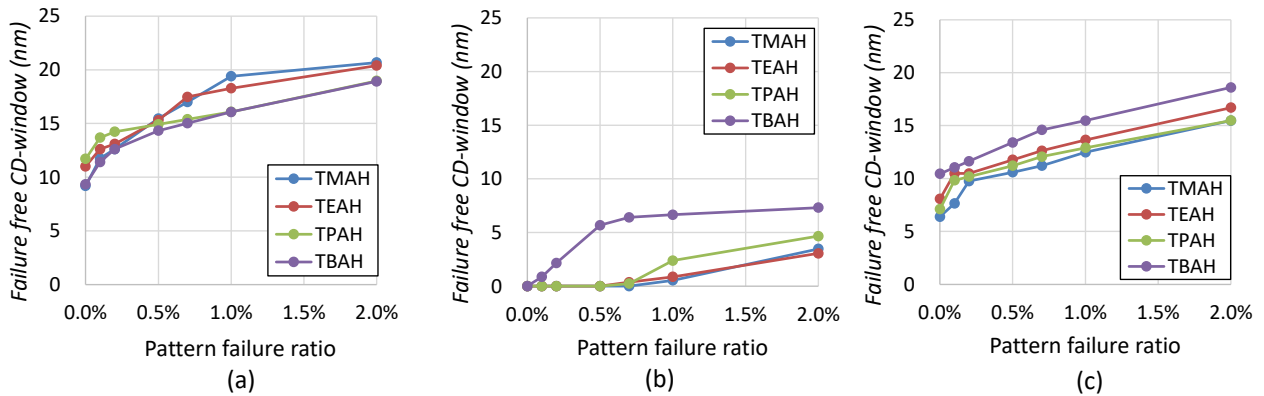


Fig. 4-5 *Failure free CD-window* at various pattern failure ratios for (a) PHS-, (b) acryl-, and (c) hybrid-type photoresists in various developer solutions (TMAH, TEAH, TPAH, and TBAH).

4-3-2. Effect of alkyl chain length of tetraalkylammonium hydroxide on *failure free CD-window*

In the case of the PHS-type photoresist, the dissolution agent contains phenolic hydroxyl groups.³⁷⁾ It has been reported that the dissolution dynamics of the PHS-type photoresist did not depend on the alkyl chain length. It was suggested that the penetration of tetraalkylammonium cations into the resist film and the dissociation of the resist polymer were not affected by the alkyl chain length.³⁴⁾ In the low-pattern-failure-ratio region (<0.5%), the *failure free CD-window* did not significantly depend on the alkyl chain length. This corresponds to the trend of dissolution kinetics observed in our previous study.³⁴⁾ In the high-pattern-failure-ratio region (>0.5%), the *failure free CD-window* for TMAH and TEAH was larger than that for TPAH and TBAH. In this case, the *failure free CD-window* decreased owing to the increase in the number of open CH defects. This means that the resist patterns (unexposed region) at a high exposure dose are susceptible to undesired polymer dissolution. In such areas of the

resist film (at which the impact of chemical blur and/or photon shot noise phenomena generate a large partially exposed area that may reach the spaces between CH patterns), the resist polymer is considered to be partially deprotected. As reported elsewhere³⁸⁾, the use of long alkyl chain developer is assumed to affect the wettability characteristics of these partially deprotected resist surfaces. Surface wettability (contact angle) measurements of resist surfaces at various EUV exposure doses have shown that; at low exposure doses the wettability of PHS-type resist surfaces to both TMAH and TBAH are relatively the same. However, when exposure dose is increased, PHS-type resist surfaces exhibit a relative increase in hydrophobicity (increase in contact angle) for the samples applied to TMAH developers. At the same exposure doses, a relative increase in hydrophilicity (decrease in contact angle) was observed for the samples applied to TBAH developers.³⁸⁾ The authors of Ref. 38 speculated that the higher hydrophobicity for TMAH may be caused by surface roughening, rather than a change in chemical nature of the surface. Our results suggested a change in chemical properties of the surface (We do not deny the surface roughening). Such changes in wettability, namely, the changes in polar and nonpolar components may have promoted the dissolution of the partially deprotected region in TBAH developers, resulting in an increase in open CH defects.

In the case of the acryl-type photoresist, the smaller the alkyl length of tetraalkylammonium hydroxide, the larger the number of stochastic defects (both closed and open CH defects), resulting in a small *failure free CD-window*. The dissolution agent in the acryl-type photoresist is carboxylic acid, unlike that in the PHS-type photoresist. The pK_a of carboxylic acids is lower than that of phenolic hydroxyl groups. The alcoholic hydroxyl groups were incorporated promoting water intake, because the molecular structure of the acryl-type photoresist is too hydrophobic without the alcoholic hydroxyl groups to be used as a resist polymer. Because the alcoholic hydroxyl groups are not dissociated in alkaline developers, their contribution to polymer dissolution is smaller than that of acidic units. It has been reported that such properties of acryl-type photoresists induced a marked swelling during development in the order to TMAH>TEAH>TPAH>TBAH.³⁴⁾ The increase in the number of stochastic defects shown in Fig. 3 (in comparison with PHS-type photoresist) is considered to be due to the enhanced swelling of the acryl-type photoresist during dissolution. The dissolution characteristic of acryl-type photoresist particularly impacted closed CH defects. Specifically, it is assumed that during CH pattern formation in developers, the partially exposed inner walls of the CH pattern reach

a point where the swollen sections reach high proximity or come in contact with the inner walls on the opposite side, increasing the probability of formation of closed CH defects. The number of open CH defects increased when short-alkyl-chain developers were utilized. Earlier reports indicated that with the TMAH developer, large swelling and an increase in dissolution speed was observed with the acryl-type resist³⁴). This phenomenon is further confirmed by the observed solubility (as evidenced by the occurrence of open CH defects) of the acryl-type resist even in the low exposure dose conditions (Fig. 4-3(b)). For this reason, given the same exposure dose condition, acryl-type resist will be more soluble in TMAH compared to TBAH, thus resulting in increased open CH defects. Moreover, it is also noteworthy that the order of *failure free CD-window* among the four developers roughly corresponded to the inverse order of swelling. The *failure free CD-window* increased with the reduction of swelling during development.

In the case of the hybrid-type photoresist, the developer with a tetraalkylammonium hydroxide with a long alkyl chain resulted in a large *failure free CD-window* (mostly due to the reduction of open CH defects). This is different from the results obtained with the PHS-type photoresist where open CH defects increased when a long alkyl chain developer was utilized. Considering these results, the following assumptions were formulated.

Photoresists are made up of polar (hydrophilic) and non-polar (hydrophobic) interacting components. For photoresists to be dissolved in the alkali developer, the photoresist needs to be polar (hydrophilic). If the photoresist is having both polar and non-polar components (an original state), dissolution will not happen. Exposure changes non-polar components into polar ones and after reaching a certain threshold, dissolution will occur. However, it is still necessary for the dissolution of exposed resist films to break both polar and non-polar interactions between polymer molecules. If we categorize the three types of photoresists evaluated here in terms of non-polarity (hydrophobicity), the acryl-type resist will be the most non-polar, followed by the hybrid-type and lastly, the PHS-type resist. The hybrid-type resist which is relatively more non-polar (hydrophobic) than the PHS-type resist, has affinity to a long alkyl chain length developer i.e., relatively non-polar (hydrophobic) TBAH developer. This allows the hydrophobic interaction to be easily broken. However, *failure free CD-window* was larger in TBAH developer than in TMAH developer. Therefore, we considered the polar interaction. After exposure, the phenolic hydroxyl groups are produced from the PHS-type resist and are dissolved

during the development process. Meanwhile, carboxyl group and phenolic hydroxyl groups are produced from the hybrid-type resist and get dissolved during the development process. This suggests stronger polar interaction between the hybrid resist and developer. The polarity of tetraalkylammonium cations decrease with the increase of alkyl chain length because a long non-polar alkyl chain shields a positive charge. The relatively stronger polar interaction of the hybrid-type resist in the TMAH developer is assumed to be the reason for increased open CH defects at high exposure dose region in this material and developer condition.

4-4. Conclusion

The effects of the alkyl chain length of tetraalkylammonium hydroxide on stochastic defect generation (*failure free CD-window*) were investigated. From EUV patterning results, it was found that in the case of the PHS-type photoresist, the *failure free CD-window* was not significantly affected (almost the same value) by the alkyl chain length at a low pattern failure ratio (<0.5%). In the high-pattern-failure-ratio region (>0.5%), the *failure free CD-window* for TMAH and TEAH was larger than that for TPAH and TBAH. In contrast, a clear trend in stochastic defect generation depending on developer solutions was observed in both the acryl-type and hybrid-type photoresists. For the acryl-type photoresist, a short alkyl chain resulted in the increase in the number of stochastic defects, namely, a small *failure free CD-window*. For the hybrid-type photoresist, it was observed that a long alkyl chain resulted in a large *failure free CD-window*. These results reflected the impact of developer solutions (alkyl chain length of tetraalkylammonium hydroxide) on stochastic defect generation. These results also showed the effectiveness of tetraalkylammonium hydroxide with long alkyl chain, i.e., TBAH for the development of acryl- and hybrid-type photoresists (the latter being more commonly utilized for EUV lithography).

References

- 1) E. Verhoeven, R. Schuurhuis, M. Mastenbroek, P. Jonkers, F. Bornebroek, A. Minnaert, H. Van Dijck, P. Yaghoobi, G. Fisser, P. Tayebati, K. Hummler, and R. Van Es, Proc. SPIE **11609**, 1160908 (2021).
- 2) C. Anderson, A. Alley, W. Chao, L. Conley, C. Cork, W. Cork, R. Delano, J. DePonte, M. Dickinson, G. Gaines, J. Gamsby, E. Gullikson, G. Jones, L. McQuade, R. Miyakawa, P. Naulleau, S. Rekawa, F. Salmassi, B. Vollmer, D. Zehm, and W. Zhu, Proc. SPIE **11323**, 113230B (2020).

- 3) T. Allenet, X. Wang, M. Vockenhuber, C.-K. Yeh, I. Mochi, J. G. Santaclara, L. Van Lent-Protasova, and Y. Ekinci, Proc. SPIE **11609**, 116090J (2021).
- 4) Z. Tasdemir, X. Wang, I. Mochi, L. van Lent-Protasova, M. Meeuwissen, R. Custers, G. Rispens, R. Hoefnagels, and Y. Ekinci, Proc. SPIE **10809**, 108090L (2018).
- 5) A. Lio, Proc. SPIE **9776**, 97760V (2016).
- 6) R. -H. Kim, Proc. SPIE **10957**, 1095706 (2019).
- 7) J. van Schoot, S. Lok, E. van Setten, R. Maas, K. Troost, R. Peeters, J. Finders, J. Stoeldraijer, J. Benschop, P. Graeupner, P. Kuerz, and W. Kaiser, Proc. SPIE **11517**, 1151712 (2020).
- 8) L. de Winter, T. Tudorovskiy, J. van Schoot, K. Troost, E. Stinstra, S. Hsu, T. Gruner, J. Mueller, R. Mack, B. Bilski, J. Zimmermann, and P. Graeupner, Proc. SPIE **11517**, 1151715 (2020).
- 9) L. Wischmeier, P. Graeupner, P. Kuerz, W. Kaiser, J. van Schoot, J. Mallmann, J. de Pee, and J. Stoeldraijer, Proc. SPIE **11323**, 1132308 (2020).
- 10) E. van Setten, G. Bottiglieri, J. McNamara, J. van Schoot, K. Troost, J. Zekry, T. Fliervoet, S. Hsu, J. Zimmermann, M. Roesch, B. Bilski, and P. Graeupner, Proc. SPIE **10957**, 1095709 (2019).
- 11) P. De Bisschop and E. Hendrickx, Proc. SPIE **11323**, 113230J (2020).
- 12) M. Sanchez, G. Wallraff, N. Megiddo, and W. D. Hinsberg, Proc. SPIE **11147**, 1114717 (2019).
- 13) P. De Bisschop, J. Micro/Nanolithogr. MEMS MOEMS **17**, 041011 (2018).
- 14) T. Kozawa, J. J. Santillan, and T. Itani, Jpn. J. Appl. Phys. **53**, 066504 (2014).
- 15) R. L. Brainard, P. Trefonas, J. H. Lammers, C. A. Cutler, J. F. Mackevich, A. Trefonas, and S. A. Robertson, Proc. SPIE **5374**, 74 (2004).
- 16) J. J. Biafore, M. D. Smith, C. A. Mack, J. W. Thackeray, R. Gronheid, S. A. Roberson, T. Graves, and D. Blankenship, Proc. SPIE **7273**, 727343 (2009).
- 17) S. Fujii, T. Kozawa, K. Okamoto, J. J. Santillan, and T. Itani, Jpn. J. Appl. Phys. **54**, 086502 (2015).
- 18) T. Kozawa, J. J. Santillan, and T. Itani, Jpn. J. Appl. Phys. **52**, 076502 (2013).
- 19) T. Kozawa, J. J. Santillan, and T. Itani, Jpn. J. Appl. Phys. **53**, 084002 (2014).
- 20) T. Kozawa, J. Appl. Phys. **54**, 016502 (2015).
- 21) A. Nakajima, M. Hoshino, M. Hashimoto, and T. Kozawa, Jpn. J. Appl. Phys. **58**, 020909 (2019).
- 22) K. Nishikori, K. Kasahara, T. Kaneko, T. Sakurai, S. Dei, K. Maruyama, and R. Ayothi, Proc. SPIE **11326**, 1132612 (2020).
- 23) K. -W. Choi, V. M. Prabhu, K. A. Lavery, E. K. Lin, W.-L. Wu, J. T. Woodward, M.J. Leeson, H. B. Cao, M. Chandhok, G. Thompson, Proc. SPIE **6519**, 651943 (2007).
- 24) T.-Y. Chu and K.-P. Cheng, Proc. SPIE **3678**, 448 (1999).
- 25) M. Touky, B. Maxwell, and S. Chanthalya, Proc. SPIE **3678**, 721 (1999).
- 26) J. J. Santillan, M. Harumoto, H. Stokes, C. Mori, Y. Tanaka, Y. Arisawa, T. Motono, M. Asai, and T. Itani, Proc. SPIE **11323**, 113231W (2020).
- 27) D. Goldfarb and B. Kumar, Proc. SPIE **10586**, 1058604 (2018).
- 28) K. Petrillo, G. Huang, D. Ashworth, J. Georger, L. Ren, K. Cho, W. Montgomery, and S. Wurm, Proc. SPIE **7969**, 796913 (2011).

- 29) M. Harumoto, K. Shigemori, A. Hisai, M. Asai, and K. Kaneyama, Proc. SPIE **7636**, 76362Z (2010).
- 30) T. Itani and J. J. Santillan, J. Vac. Sci. Technol. B **27**, 2986 (2009).
- 31) J. J. Santillan, M. Harumoto, T. Motono, A. F. Santos, C. Mori, Y. Tanaka, H. Stokes, M. Asai and T. Itani, Jpn. J. Appl. Phys. **60**, SCCC01 (2021).
- 32) A. Rao, S. Kang, B. D. Vogt, V. M. Prabhu, E. K. Lin, W. -L. Wu and M. Muthukumar, Langmuir **22**, 10009 (2006).
- 33) V. M. Prabhu, R. L. Jones, E. K. Lin, C. L. Soles, W. -L. Wu, D. L. Goldfarb and M. Angelopoulos, Proc. SPIE **5039**, 404 (2003).
- 34) M. Harumoto, J. J. Santillan, T. Itani, and T. Kozawa, Jpn. J. Appl. Phys. **61**, 056506 (2022).
- 35) M. van de Kerkhof, H. Jasper, L. Levasier, R. Peeters, R. van Es, J. -W. Bosker, A. Zdravkov, E. Lenderink, F. Evangelista, P. Broman, B. Bilski, and T. Last, Proc. SPIE **10143**, 101430D (2017).
- 36) P. De Bisschop, J. Micro/Nanolith. MEMS MOEMS **16**, 041013 (2017).
- 37) N. Tanaka, K. Matsuoka, T. Kozawa, T. Ikeda, Y. Komuro, and D. Kawana, Jpn. J. Appl. Phys. **61**, SD1016 (2022).
- 38) R. Gronheid, J. Vac. Sci. Technol. B **28**, C6S1 (2010).

Chapter 5

Conclusions

Various types of defects are generated post development in EUV lithography. This work focused on understanding stochastic defects (e.g. pattern collapse, closed and open hole defects), their generation and reduction.

In Chapter 2, investigations on the reduction of pattern collapse were carried out by depressurizing the atmosphere during the deionized water rinse and drying process in the development process. The differential pressure P between the atmosphere pressure $P_{atmosphere}$ and the rinsing liquid pressure P_{rinse} is expressed as

$$P = P_{atmosphere} - P_{rinse} = \frac{2\gamma \cos \theta}{d},$$

where γ is the surface tension of rinsing liquid, θ is the contact angle with the photoresist pattern and the rinsing liquid, and d is the width of space between line patterns. Therefore, the contact angle θ is expected to increase when the atmosphere is depressurized. On the other hand, the tensile stress σ which causes pattern collapse is expressed as

$$\sigma = \frac{6\gamma \cos \theta}{d} \left(\frac{H}{L}\right)^2,$$

where H is the pattern height and L is the line width. Therefore, an increase in contact angle θ leads to a pattern collapse mitigation due to a decrease in tensile stress. In actual patterning experiments, it was shown that the line-width-without-pattern-collapse was reduced by depressurizing the development chamber. This shows that the tensile stress on the pattern was reduced. The temperature dependency and pressure dependency of the contact angle have been reported elsewhere. This research demonstrates that the contact angle between the rinse and the pattern may have been a factor in the reduction of pattern collapse by depressurization. However, the resist patterning experiments using a 45-nm 1:1 lines/spaces (L/S) pattern did not show any reduction in pattern collapse. Thus, it remains to be determined whether further pressure reduction will have an effect, or whether the photoresist dissolution behavior during development has a larger impact. Chapter 2 shows that the latter may be true.

In Chapter 3, the dissolution dynamics of three types of EUV photoresists was observed by the quartz crystal microbalance (QCM) method using four different developer solutions with different alkyl chain lengths. For poly(4-hydroxystyrene) (PHS) type photoresists, there were no significant differences from the dissolution dynamics in developers with different alkyl chain lengths. On the other hand, differences in dissolution dynamics depending on developer were observed for acryl-type

and hybrid-type photoresists. In acryl-type photoresists, TMAH which has the shortest alkyl chain length (among the developers in this experiment) and small cation, was found to cause significant swelling in the early stages of development. This is thought to be because the OH group in 3-hydroxy-1-adamantylmethacrylate of acryl-type photoresist does not dissociate in the developer solution but swells by taking in water. The smaller the cation, the more easily it is taken in. Hybrid photoresists showed faster dissolution in TBAH developer with long alkyl chains. This is because 2-methyl-2-adamantyl methacrylate is a nonpolar group, and the long alkyl chains are effective in cleaving hydrophobic interactions. This chapter reveals that the dissolution dynamics were significantly depended on the combination of EUV photoresists and developers with different alkyl chain lengths.

In Chapter 4, the effects of the alkyl chain length of tetraalkylammonium hydroxide on stochastic defect generation (failure free CD-window) were investigated. From EUV patterning results, it was found that in the case of the PHS-type photoresist, the failure free CD-window was not significantly affected (almost the same value) by the alkyl chain length at a low pattern failure ratio ($<0.5\%$). In the high-pattern-failure-ratio region ($>0.5\%$), the failure free CD-window for TMAH and TEAH was larger than that for TPAH and TBAH. In contrast, a clear trend in stochastic defect generation depending on developer solutions was observed in both the acryl-type and hybrid-type photoresists. For the acryl-type photoresist, a short alkyl chain resulted in the increase in the number of stochastic defects, namely, a small failure free CD-window. For the hybrid-type photoresist, it was observed that a long alkyl chain resulted in a large failure free CD-window. These results reflected the impact of developer solutions (alkyl chain length of tetraalkylammonium hydroxide) on stochastic defect generation. These results also showed the effectiveness of tetraalkylammonium hydroxide with long alkyl chain, i.e., TBAH for the development of acryl- and hybrid-type photoresists (the latter being more commonly utilized for EUV lithography).

Finally, this study clarified that aside from the photoresist material, the drying process and alkaline developer materials play a significant role in stochastic defect generation in EUV lithography. This work has also shown that for the fabrication of much finer patterns in the future, the research and development of EUV photoresist materials, and the advancement of developer materials (that are less likely to cause swelling) will also be necessary. Furthermore, with new technological trends pointing towards the use of organic solvents as developer materials for next generation photoresists, such as

metal oxide photoresists or main chain scission photoresists, the importance of research on photoresist dissolution process is obvious. For this purpose, the method established here is viewed effective in clarifying the relationship between dissolution behavior and stochastic defects generation. The results obtained in this thesis can lead to pointers in achieving the optimal combination of photoresist and developer materials.

List of publications

1. Pattern collapse mitigation by controlling atmosphere during development process for semiconductor lithography
Masahiko Harumoto, Tomohiro Motono, Andreia Figueiredo dos Santos, Chisayo Mori, Yuji Tanaka, Harold Stokes, Masaya Asai, Julius Joseph Santillan, Toshiro Itani, and Takahiro Kozawa
Jpn. J. Appl. Phys. **60**, SCCA03 (2021).
2. Dependence of photoresist dissolution dynamics in alkaline developers on alkyl chain length of tetraalkylammonium hydroxide
Masahiko Harumoto, Julius Joseph Santillan, Toshiro Itani, and Takahiro Kozawa
Jpn. J. Appl. Phys. **61**, 056506 (2022).
3. Stochastic defect generation depending on tetraalkylhydroxide aqueous developers in extreme ultraviolet lithography
Masahiko Harumoto, Andreia Figueiredo dos Santos, Julius Joseph Santillan, Toshiro Itani, and Takahiro Kozawa
Jpn. J. Appl. Phys. **62**, 016503 (2023).

Acknowledgement

I would like to express my deepest appreciation to Prof. T. Kozawa for his guidance throughout this work.

I'm also extremely grateful to Prof. N. Imanaka and Prof. A. Saeki, of the Division of Applied Chemistry, Graduate School of Engineering in Osaka University, for reviewing this thesis and giving their valuable comments and suggestions. I also would like to acknowledge Prof. T. Itani and Assoc. Prof. J. J. Santillan at SANKEN, Osaka University for their cooperation in conducting the experiments.

I would also like to extend my sincere thanks to my colleagues; Dr. H. Stokes, Dr. N. Frolet, Dr. A. Santos, Mr. H. Marhfour and Mr. W. Zanders for the invaluable support in preparing the photoresist pattern samples, and Mr. Y. Tanaka, Ms. C. Mori, Mr. Y. Arisawa, Dr. T. Motono and Mr. M. Asai for the kind cooperation and very useful advice.

I would also like to recognize the members in Kozawa Lab; Assoc. Prof. Y. Muroya, Asst. Prof. K. Okamoto, Prof. K. Kobayashi, Asst. Prof. A. Nakajima, Ms. Y. Ito, Ms. Y. Sasaki, Ms. K. Matsuoka, Ms. K. Watanabe, Ms. K. Watanabe (our secretary), Mr. A. Konda, Mr. Y. Ikari, Mr. N. Maeda, Mr. K. Azumagawa, Mr. K. Ikeuchi, Ms. T. Otsuka, Mr. N. Tanaka, Ms. Y. Jin, Ms. Y. Takata, Ms. H. Betsumiya, Mr. Y. Iwashige, Mr. J. Wang, Ms. Y. Tsuda and Mr. S. Nishimoto for the warm welcome and the wonderful new memories of being a student again.

Finally, I would like to extend deep gratitude to my family, especially my wife Akiko, my son Kazuki and daughter Mari for the love, understanding, and patience.